Air distribution in street canyons: a CFD study

Report

Author: Jordi Galí Gimeno

Director: Ivette Maria Rodríguez Pérez

Date: 10 June 2019

Universitat Politècnica de Catalunya. UPC

The School of Industrial, Aerospace and Audiovisual Engineering of Terrassa. ESEIAAT

Bachelor's degree in Aerospace Vehicle Engineering

UNIVERSITAT POLITÈCNICA DE CATALUNYA
BARCELONATECH

Escola Superior d'Enginyeries Industrial, Aeroespacial i Audiovisual de Terrassa

[This page intentionally left blank]

1 Abstract

Heat island effect and air quality are major issues in big cities and the shape of the street canyons is directly related with these problems. The only presence the buildings modifies the temperature in their surroundings because of the direct interference with radiation, moisture and wind. However, the main reason why buildings affect temperature is because of the interference with the airflow. Therefore, a study of the air through the street canyons must be done. This computational fluid dynamics (CFD) study will be made with open source programs. To validate our model a 2D case will be solved and the results will be compared with the experimental data from the Bibliography. Once the model is validated, a 3D geometry will be solved in order to study the case proposed. In this late geometry the fact that the airflow passes through the buildings sideways will be considered. Then, the effect of the presence of buildings and the geometry of street canyons on the temperatures in cities will be discussed.

Contents

List of Figures

List of Tables

2 Introduction

2.1 Aim

The main objective of the project is the study of flow distribution in idealized street canyons. Doing this, the relation between the temperature in cities and the geometry of street canyons will be shown. The purpose of this project is also to see how the pollutant dispersion changes with the city geometrical distribution.

2.2 Scope

To be able to reach the main objective it will be necessary for the student to develop skills on computational fluid dynamics (CFD). Developing skills on visualization, meshing and programming for post-processing results. The solver program will be $OpenFoam6$, to create the mesh $Gmsh$ will be used and, finally, to visualize the results, $paraview56$. Once the simulation is done, its the results will be processed with $Matlab2018a$. Not only it will be important to learn how to use the programs, but also how to apply the boundary conditions to the case studied. Therefore, it will be necessary to learn about the turbulence models, with special attention to the Reynolds-averaged Navier-Stokes (RANS) model. As a last step, a state of the art of the simulation of street canyons must be done.

2.3 Requirements

To complete the study, some requirements must be fulfilled. The following are the ones proposed at the beginning of the project. At the end, it will be necessary to make clear if they have been fulfilled. This way, if one objective is not well reached, a justification of this result will be done. The requirements are placed in chronological order so when one objective is reached, it will be possible to continue with the following. The first requirement is to define the base case to be simulated. The second, is to make a model refinement study on the base case. The third one is the most important requirement of the first part. It consist of validating the base case with results from the literature. Once this is achieved, a three-dimension study to analyze the influence of the length of the canyon and the tip vortex effects must be performed. After that, a comparison between the two and three dimension cases. The last requirement is to deliver the report on the 10th of June.

2.4 Background

Air distribution in street canyons is very important in modern cities where heat island effect and air quality are major issues. A simplified model of street canyons with buildings of the same height and separated by the same distance will be studied. When this is completed, it will be possible to verify the model with experimental data from the literature. The use of this study is to be able to see how the fluid behaves in a three dimensional geometry.

2.5 Acknowledgments

After this project, I want to give special thanks to the director Ivette. If modeling the turbulence is a complicated issue, explaining it is even harder. So huge thanks for the meetings where all the doubts and questions have been solved. This project has served to see how big and complicated the world of modelling the flow is. And to Navid, for helping during the firsts steps with fluid problem solving. Thanks to him, the world of a fluid solver like Openfoam started to make sense.

3 Theoretical introduction

3.1 General description of the problem

The focus of this thesis is to study the effect of the airflow in modern cities. And this will be conditioned mainly by buildings' geometry. So before entering with the relation between the airflow and the geometry of the city, the problem must be studied from a general point of view.

The geometry of the city can provide information of some characteristics that will be an improvement for the quality of life of citizens. These characteristics can also be called objectives for a good city planning. The first one is to maximize the shelter that buildings give to pedestrians to reduce the impact of heavy winds or gusts that can blow them over. This is also very important for cities where snowstorms are frequent. Another objective is to maximize the dispersion of air pollutants. Pedestrians and cars coexist most of the time, so being exposed to all this contaminated air is a major health problem not only for pedestrians, but also for the people who live in the buildings. The third objective is to maximize the urban heat island effect. This will be very favourable to nights or to cities located *near* the poles. On the contrary, for cities located *near* to the equator the objective is to reduce this effect. Finally, the last objective is to maximize the solar access.

However, obtaining all four objectives is a difficult task. The main reason is because the two first ones are in conflict: in order to ensure a good shelter, buildings must be placed very close to each other and in order to obtain a good dispersion of the air pollutants, streets must be very open. The same problem exists with the two last objectives. If streets are very closed, they will ensure a good heat island effect but the solar access will be very limited [1]. Here, the goal is not to study if one objective is more important than another. And either is to find the best geometry so as to reach the best city planning. This will serve as a reference, but in the problem, the main goal is to reduce the heat island effect and maximize the dispersion of air pollutants.

Qualitatively it is possible to see that a group of buildings will cause an impact on radiation heat transfer. Some parts of the buildings will receive it directly from the sun, other parts will receive the radiation from the reflection of the sunlit walls and other surfaces will receive less radiation when they are located at the shadow, as seen in figure 1.

Talking about the details of the study, if the focus is the airflow on cities,

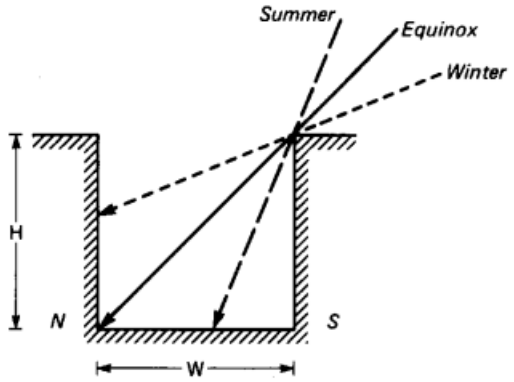

Figure 1: Angles of incidence of direct beam solar radiation in an E-W canyon, in a city at 45^o. In a canyon with AR=1. (extracted from: [1])

there are a huge amount of things that could be considered. Taking *el barri de l'Eixample* in Barcelona as an example, one could see that the trees are going to have an important role. It is very easy to see that having a row of trees along the street will interfere with the air. Having a street where cars and buses travel during most of the time will cause a disturbance on the air. Not only by increasing the air temperature with the combustion, but also by leaving a turbulent wake. Also, if the street is one way road, the longitudinal velocity component of the air will be reinforced. To complete the analysis, other small details such as balconies or imperfections in the geometry can be considered. Nevertheless, none of these details will be considered in this study for simplicity reasons.

3.2 Urban Geometry

As it is commented before, the main goal in this study is to analyze how the geometry of the buildings increases or decreases the heat island effect. It is worth noting that the effect of convective heat transfer from the wind is very notorious. In fact, buildings acting as an obstacle to the wind will be the main reason of temperature modification [2]. For that reason, the radiation from the sun will not be considered in this study. How the flow state is modified because of the city geometry will be the main goal.

The pattern of the wind around a building is shown in figures (2) and (3).

As is shown in figures, the front of the buildings are located normal to the flow velocity. In the study, they will be also placed normal to the airflow

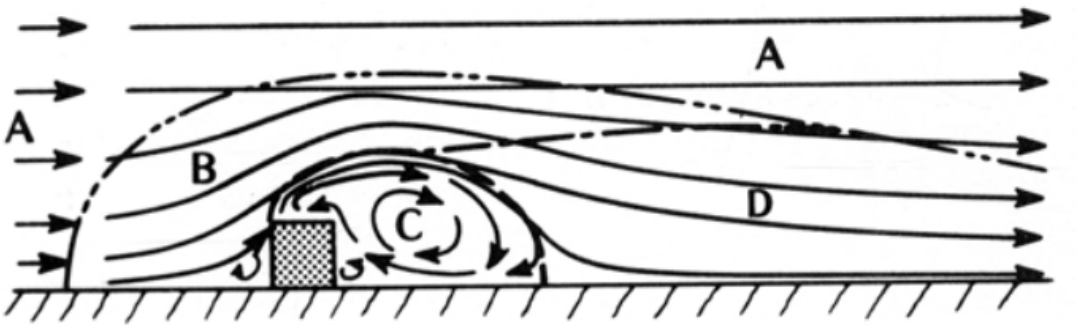

Figure 2: Side view of the air around a building (extracted from: [2])

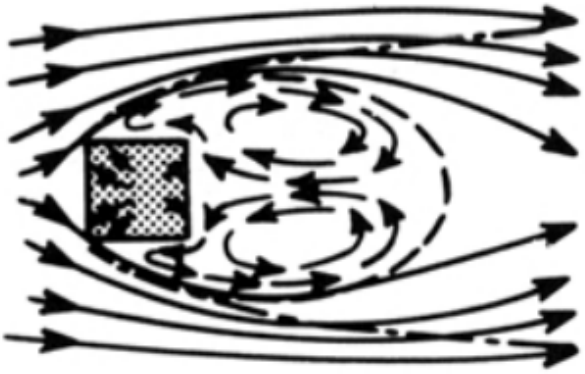

Figure 3: Aerial view of the air around a building (extracted from: [2])

for many reasons. The first one is that the experiment used to validate the model will also be the study of the airflow around buildings placed normal to the air. Another reason is that this geometry simplifies the study.

As seen in figure (2) there are four zones of study. A is the zone where the air is not disturbed so the other three ones suffer the effect of the building. Zone B is where the air is displaced. There the point of maximum pressure is found at the front of the building, and it is called a stagnation point. Region C is clearly the zone where most turbulence is found, since pressure is low and is hard to know the path of the streamlines. This is also called the *suction* zone. D zone is the wake, also called sometimes the tail. In this zone, the flow still suffers from the effect of the turbulence and its velocity is lower than the velocity in the region A.

Since the study is focused in an urban area, the geometry parameters which will be used must be defined. In order to do that, the aspect ratio is used.

The aspect ratio of the buildings in an urban area will be $AR = H/W$ being H The height of the buildings and W the distance between them.

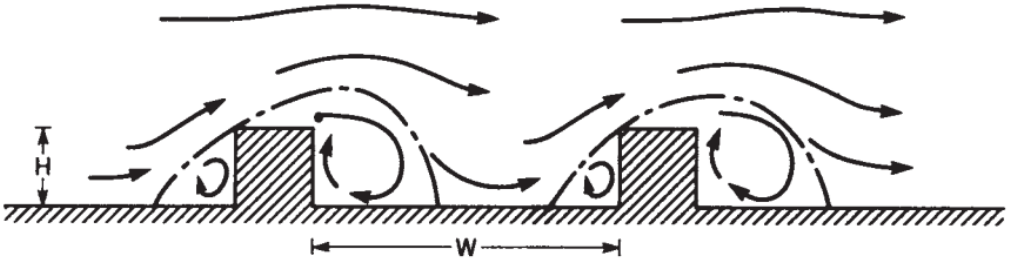

Figure 4: Lateral view of an urban area of AR = 0.4 (extracted from: [2])

For an urban area of $AR < 0.4$ the effect will be more or less the same as if the buildings where isolated [2] (As shown in figure 4).

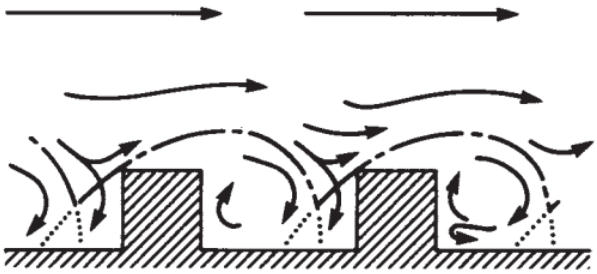

Figure 5: Lateral view of an urban area of AR = 0.7 (extracted from: [2])

If the aspect ratio in the urban area is $AR < 0.7$, the wake of the buildings will interfere with the displaced zone of the next building. It is easy to see that effect in figure 5. The flow streamlines become harder to predict because of this interference.

For higher aspect ratio buildings than the unit $AR > 1$, the air behaves as shown in figure 6. The main fluid streamlines flows over the buildings while in the space between them, the *streets*, there is a vortex.

Another parameter that will be used is the relation between the length of the building (normal to the flow) L and the distance between buildings L/W. In figure 7, the geometry parameters are shown.

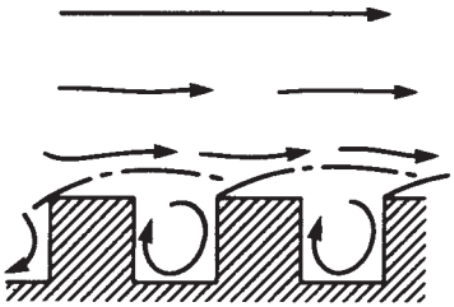

Figure 6: Lateral view of an urban area of AR = 1 (extracted from: [2])

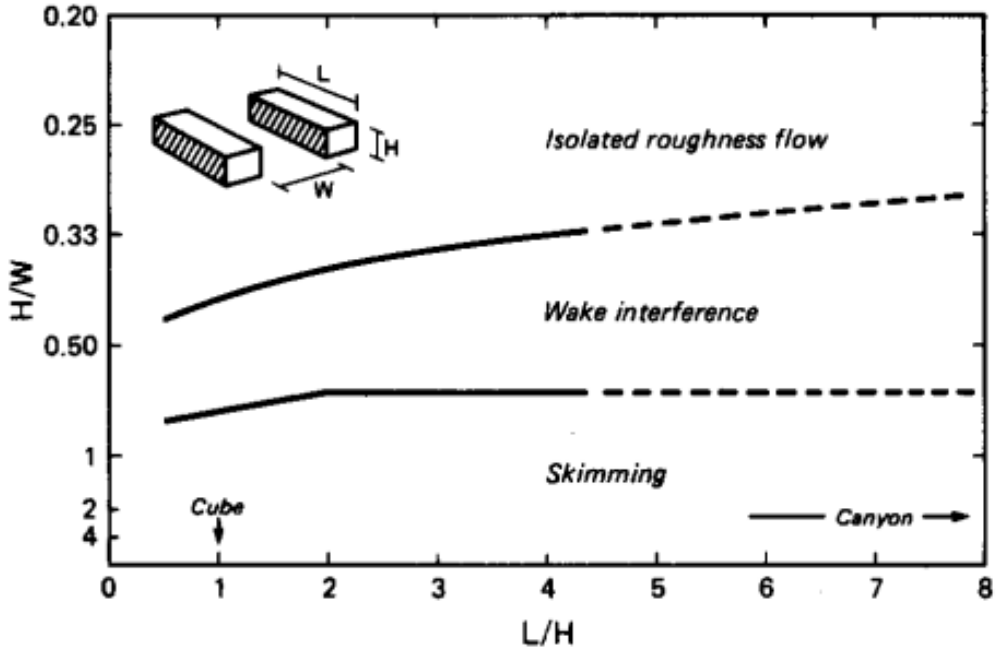

Figure 7: Lines dividing the flow into three regimes (extracted from: [1])

The study will focus mainly on the skimming zone.

Before entering into the mathematical description, the flow must be defined in the case studied. In cities, the fluid is air at very low velocities and this is why this study does not focus on heavy winds or gusts. Is a three dimension exterior flow, Newtonian, incompressible and homogeneous. As the fluid is turbulent, it will be studied as a non-stationary case. However, the turbulence in this case is very small as will be seen later.

General laws of continuum mechanics are used to describe the flow state: conservation of mass, conservation of momentum and conservation of energy[6]. The fluid is expressed as a particle in movement which has two different mathematical representations, the Lagrangian and Eulerian models. In the Lagrangian representation the fluid particle state is described in reference to its initial position. And the Eulerian (the one used), describes the state of the particle in reference of its position in space and time.

3.3 Solving fluid problems

To be able to solve the problem defined before, it is worth taking a look on the possible tools to do it. Until 1960, all solutions were analytical or empirical [7].

To get to an empirical solution, huge and expensive infrastructures are needed. And in our case the street canyon is so big that it would be impossible to build a laboratory for this purpose. During the first half of the 20th century, engineers built laboratories at scale to model problems for large geometries. But it was not easy because they had to establish some "laws" to scale the solution the experiment gave to the geometry of the problem. They had to adapt the flow properties to give a correct answer.

As it is commented before, the fluid is very hard to describe mathematically. There is an enormous number of flow particles that are in contact with each other. If a flow particle suffers a change to its state, like a change in velocity or pressure, this will affect all the particles next to the first one. Thus, an analytical solution is rarely possible mainly because of the complexity of the equations used to define the flow state. First of all the flow is three dimensional, which means that all the variables change through space so equations must be solved for each axis in the three directions. The velocity flow, the temperature and pressure fields must be calculated and the flow properties must be considered at each point in space. If the geometry is very simple sometimes the assumption that the flow is one dimensional can be made. This simplifies the problem, but the solution will carry an error. Another reason is that the equations are strongly coupled, the velocity is very related to the pressure and vice versa. And finally, the equations used to solve the flow state are not linear as will be shown after. The Navies Stokes equations are partial differential equations that must be simplified to ordinary differential equations to solve them by integration [7]. The solution to an analytical procedure is exact and continuous, it can be defined at every point of space.

To solve the flow dynamics problems, the method used nowadays is numerical. Numerical methods are discrete so the space is divided in a certain number of points called nodes. After this, the Navier-Stokes equations must be integrated at each node. In this case, partial differential equations are not converted into ordinary differential equations. Integrating the equations at each node means that the equations are converted from partial differential equations to algebraic equations. This process is called discretisation [7].

3.4 Navier-Stokes equations

If the fluid is Newtonian, the viscous stresses and the strain rate are proportional. Incompressible means that the flow is working in a low velocity range (less than 0.3 Mach velocity), and if the fluid is also homogeneous, the density is constant in all the control volume during all the period of time $\rho(x,t) = \rho_0$. In this study, because of that, it will be defined from now on as $\rho = \rho_0$.

The mass conservation equation for a fluid can be expressed as follows[6]:

$$\frac{\partial \rho}{\partial t} + \rho \frac{\partial u_i}{\partial x_i} = 0 \tag{1}$$

But as it is mentioned before, the incompressible and homogeneous fluid condition must be applied so the equation (1) is rewritten as:

$$\frac{\partial u_i}{\partial x_i} = 0 \tag{2}$$

This is the conservation of mass equation used in this study. It says that the mass can not be created or destroyed in our control volume and that the mass flow throughout the inlet section is the same mass flow throughout the outlet section. As it is a three dimension flow the velocity is described as $U = (u, v, w)$.

The conservation of momentum is expressed as the well known second Newton's law:

$$\sum F = ma \tag{3}$$

For a fluid, the equation can be written as [4]:

$$\rho\{\frac{\partial u_i}{\partial t} + u_i \frac{\partial u_i}{\partial x_j}\} = -\frac{\partial p}{\partial x_i} + \frac{\partial \tau_{ij}}{\partial x_j} + f \tag{4}$$

Where $\tau_{ij} = 2\mu s_{ij}$, being τ_{ij} the viscous stress tensor and:

$$s_{ij} = \frac{1}{2}(\frac{\partial u_i}{\partial x_j} + \frac{\partial u_j}{\partial x_i}) \tag{5}$$

Where μ is the shear viscosity coefficient and s_{ij} is the strain-rate tensor. f is the body or volume force, in this case it represents the force that the gravity makes over the fluid particle. The gravity can be neglected without making a large error. The system composed by (4) and (2) was proposed by M. H. Navier in 1827, and later in 1845, Strokes found a satisfactory justification on the basis of the continuum mechanics approach [8].

The time-averaging process must be simplified by rewriting the convective term in conservation form [4]:

$$u_j \frac{\partial u_i}{\partial x_j} = \frac{\partial}{\partial x_j}(u_j u_i) - u_i \frac{\partial u_j}{\partial x_j} = \frac{\partial}{\partial x_j}(u_j u_i) \tag{6}$$

Then combining (4) and (6) the Navier-Stokes equation in conservative form is obtained[4]:

$$\rho \frac{\partial u_i}{\partial t} + \rho \frac{\partial}{\partial x_j}(u_j u_i) = -\frac{\partial p}{\partial x_i} + \frac{\partial}{\partial x_j}(2\mu s_{ij}) \tag{7}$$

Then the equation (7) must be averaged. This process will be done later, since first an introduction of the main fluid dynamics solvers must be done to understand the approach taken in our model. The approach of the Navier-Stokes equations used is this study will be the RNG k-epsilon. This will be discussed later.

3.5 CFD models

The main aspect that has to be clear when solving a fluid dynamics problem is that there is no model wide enough to solve the majority of cases. First of all, Navier-Stokes equations are so general that they must be derived in order to adapt them to the case studied. Each derivation will depend on the fluid characteristics. If the flow is steady for example, the simplification will lead to a more simple model in comparison with non-steady cases. In the case of turbulent flows, the model that must be applied is non-steady. Another aspect of the flow that will greatly modify the model used is the velocity. Working at very high velocities means that the flow must be considered compressible, such as modeling the air flow through an airplane. There are some suitable approaches to solve our case, like the direct numerical simulation

(DNS), the large eddy simulations (LES) and the Reynolds-averaged Navier-Stokes equations (RANS).

Solving the case with (DNS) means that every length and time scale in the domain is fully resolved. This is a very expensive way of computing the problem because the motions of turbulence appear over a wide range of scales [9].

The (LES) method uses the "filtered" equations that remove the small eddies, usually taken as the mesh size. The small scale motion of the flow is modeled. The main reason why (LES) is so used is that it gives small error computing the turbulence. However, it is also a very expensive model.

And the (RANS) model computes the average state of the flow and models the fluctuations. Reynolds averaging assumes a variety of forms involving either an integral or a summation. The three forms are time averaging, spatial averaging and ensemble averaging [4]. Time averaging is a good approach for stationary turbulence. Stationary turbulence is a turbulent flow that does not vary along time. Spatial averaging is appropriate for homogeneous turbulence, a flow that is uniform in all directions. And ensemble averaging is the summation of a determined number of identical experiments. For our case, a turbulence that is both stationary and homogeneous, the three averages must be equal.

3.6 Reynolds averaging

The best way to average a non-stationary turbulence is by time-averaging the Navier-Stokes equations. Then, the instantaneous velocity is expressed as:

$$u_i = \overline{U_i} + u_i' \tag{8}$$

Where u_i is the instantaneous velocity, U_i is the mean velocity and u_i' is the fluctuating part, also called the Reynolds stresses, as can be seen in figure 8.

To be able to continue with the mathematical derivation, it has to be clear the following step. When the product of two properties must be averaged the mathematical procedure is [4]:

$$\overline{\phi\psi} = \overline{(\Phi + \phi')(\Psi + \psi')} = \overline{\Phi\Psi + \Phi\psi' + \Psi\phi' + \phi'\psi'} = \Phi\Psi + \overline{\phi'\psi'} \tag{9}$$

This occurs because the product of a mean quantity and a fluctuation quantity has zero mean [4].

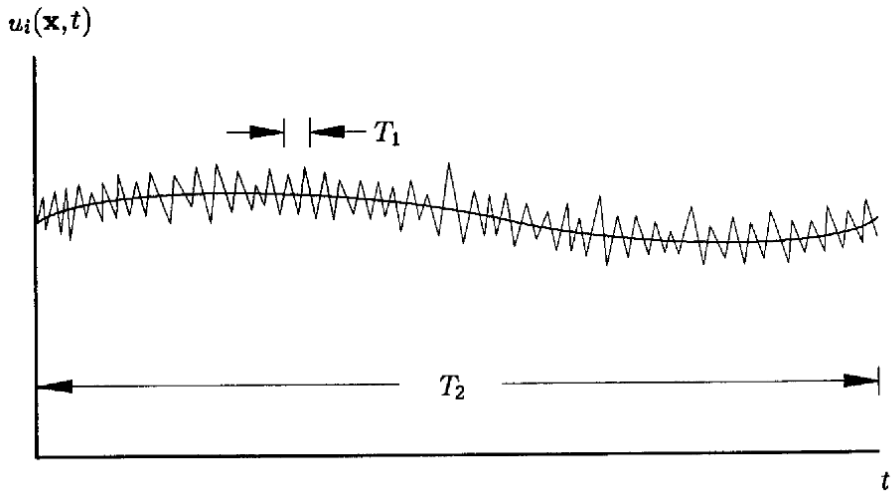

Figure 8: Time-averaging for non-stationary case (extracted from: [3])

The model used in this study has to be able to make an approach of the main velocity and the fluctuations so the Navier-Stokes equations (7) and (2) must be averaged. The solution yields to:

$$\frac{\partial U_i}{\partial x_i} = 0 \tag{10}$$

$$\rho\frac{\partial U_i}{\partial t} + \rho\frac{\partial}{\partial x_j}(U_j U_i + \overline{u_j\prime u_i\prime}) = -\frac{\partial P}{\partial x_i} + \frac{\partial}{\partial x_j}(2\mu S_{ij}) \tag{11}$$

The mass conservation equation averaged just replaces the instantaneous velocity by the mean velocity. The fluctuation part of the velocity has also zero divergence. The term that has appeared in the momentum equation $\overline{u_i' u_j'}$ is the most difficult part to calculate. Using the equation (6) as before but in the opposite direction the equation is rewritten as:

$$\rho\frac{\partial U_i}{\partial t} + \rho U_j\frac{\partial U_i}{\partial x_j} = -\frac{\partial P}{\partial x_i} + \frac{\partial}{\partial x_j}(2\mu S_{ij} - \overline{\rho u_j\prime u_i\prime}) \tag{12}$$

This equation is called the Reynolds-averaged Navier-Stokes equation [4]. Where $-\overline{\rho u_j\prime u_i\prime}$ is the Reynolds-stress tensor:

$$\tau_{ij} = -\overline{\rho u_j\prime u_i\prime} \tag{13}$$

This is a symmetric tensor so it has six independent components. This means that by averaging, six new unknown variables to the system have been introduced. If the pressure and the three velocity components are unknowns, now,

by adding the six Reynolds-stress components, the system has ten unknowns. And if our equations are the mass conservation (10) and the momentum conservation (12), which has three components, the system is not closed yet.

3.6.1 Reynolds-Stress equations

To found new equations in order to close the system, the Navier-Stokes equations are multiplied by fluctuating property and the product is averaged. If $N(u_i)$ is the Navier-Stokes operator and the viscous term has been simplified, the equation is written as:

$$N(u_i) = \rho\frac{\partial u_i}{\partial t} + \rho u_k\frac{\partial u_i}{\partial x_k} + \frac{\partial p}{\partial x_i} - \mu\frac{\partial^2 u_i}{\partial x_k \partial x_k} = 0 \tag{14}$$

The following time average is formed:

$$\overline{u_i' N(u_j) + u_j' N(u_i)} = 0 \tag{15}$$

The time-averaging process is shown term by term for clarity. The unsteady term is:

$$\overline{u_i'(\rho u_j)_{,t} + u_j'(\rho u_i)_{,t}} = -\frac{\partial \tau_{ij}}{\partial t} \tag{16}$$

The convective term is written as:

$$\overline{\rho u_i' u_k u_{j,k} + \rho u_j' u_k u_{i,k}} = -U_k\frac{\partial \tau_{ij}}{\partial x_k} - \tau_{ik}\frac{\partial U_j}{\partial x_k} - \tau_{jk}\frac{\partial U_i}{\partial x_k} + \frac{\partial}{\partial x_k}(\overline{\rho u_i' u_j' u_k'}) \tag{17}$$

The pressure gradient term yields:

$$\overline{u_i' p_j + u_j' p_i} = \overline{u_i'\frac{\partial p'}{\partial x_j} + u_j'\frac{\partial p'}{\partial x_i}} \tag{18}$$

And finally, the viscous term is written as:

$$\overline{\mu(u_i' u_{j,kk} + u_j' u_{i,kk})} = -\nu\frac{\partial^2 \tau_{ij}}{\partial x_k \partial x_k} - \overline{2\mu\frac{\partial u_i'}{\partial x_k}\frac{\partial u_j'}{\partial x_k}} \tag{19}$$

Putting all the terms back in the same equation yields:

$$\begin{aligned}\frac{\partial \tau_{ij}}{\partial t} + U_k\frac{\partial \tau_{ij}}{\partial x_k} = -\tau_{ik}\frac{\partial U_j}{\partial x_k} - \tau_{jk}\frac{\partial U_i}{\partial x_k} + \overline{2\mu\frac{\partial u_i'}{\partial x_k}\frac{\partial u_j'}{\partial x_k}} \\ + \overline{u_i'\frac{\partial p'}{\partial x_j} + u_j'\frac{\partial p'}{\partial x_i}} + \frac{\partial}{\partial x_k}(\nu\frac{\partial \tau_{ij}}{\partial x_k} + \overline{\rho u_i' u_j' u_k'})\end{aligned} \tag{20}$$

Six new equations are added to the system, one for each independent component of the Reynolds-stress tensor. However, by averaging 22 new unknowns are formed. There are ten new unknowns because of the convective term, six because of the pressure gradient term and six because of the viscous term. This shows the problem with the closure in turbulence. Mathematically, it is very complicated to ensure the closure of the problem. Until now, the process has been just mathematical, but to be able to close the system, physical principles must be added. These principles are approximations for the unknown correlations.

All the equations are obtained from [4]. The most complex derivations and algebra are not shown in this thesis but can be found in the corresponding book.

3.6.2 Turbulence energy equation model

In contrast with the algebraic models, the turbulence energy equation models have an approach to the turbulent length scale. However, the One-equation models and the Two-equation models both retain the Boussinesq eddy-viscosity approximation. The One-equation models are incomplete as they relate the turbulence length scale to some typical flow dimension but the two-equation models have an equation for this parameter [4]. The models of interest are the two-equation models.

Choosing the specific kinetic energy of the turbulent fluctuations as the basis of his velocity scale:

$$k = \frac{1}{2}\overline{u_i' u_j'} = \frac{1}{2}(\overline{u'^2} + \overline{v'^2} + \overline{w'^2}) \tag{21}$$

The parameter k should be referred as specific turbulence kinetic energy. The eddy viscosity is:

$$\mu_T = constant \rho k^{1/2} l \tag{22}$$

Being l the the turbulence length scale. To obtain k the trace of the Reynolds stress tensor is taken:

$$\tau_{ii} = -\rho\overline{u_i' u_i'} = -2\rho k \tag{23}$$

If before a differential equation has been derived (20), a corresponding equation can be derived for k. This leads to a transport equation for the turbulence kinetic energy [4]:

$$\rho\frac{\partial k}{\partial t} + \rho U_j \frac{\partial k}{\partial x_j} = \tau_{ij}\frac{\partial U_i}{\partial x_j} - \rho\epsilon + \frac{\partial}{\partial x_j}[\mu\frac{\partial k}{\partial x_j} - \frac{1}{2}\rho\overline{u_i' u_i' u_j'} - \overline{p' u_j'}] \tag{24}$$

Where ϵ is the dissipation per unit mass:

$$\epsilon = \nu \overline{\frac{\partial u_i'}{\partial x_k} \frac{\partial u_i'}{\partial x_k}} \tag{25}$$

The two terms of the left-hand of the equation (24) are the unsteady and the convection term. The first term of the right-hand side is the rate at which kinetic energy is transferred from the mean flow to the turbulence, it is called the production. The following term to the right is the dissipation of the turbulence kinetic energy. The three following terms are the molecular diffusion, the turbulent transport and the pressure diffusion, from left to right. It the goal is to ensure that the equation (24) is closed, the τ_{ij}, dissipation, turbulent transport and pressure diffusion must be specified. The Reynolds-Stress Tensor is defined at the equation (23). The turbulent transport and the pressure diffusion approach is:

$$\frac{1}{2}\rho \overline{u_i' u_i' u_j'} + \overline{p' u_j'} = -\frac{\mu_T}{\sigma_k} \frac{\partial k}{\partial x_j} \tag{26}$$

Where σ_k is a coefficient. For the dissipation, [Taylor (1935)] show that:

$$\epsilon \sim k^{3/2}/l \tag{27}$$

the equations (26) and (24) must be mixed to find the equation that is used in virtually all turbulence energy equation models [4]:

$$\rho \frac{\partial k}{\partial t} + \rho U_j \frac{\partial k}{\partial x_j} = \tau_{ij} \frac{\partial U_i}{\partial x_j} - \rho\epsilon + \frac{\partial}{\partial x_j}[(\mu + \mu_T/\sigma_k)\frac{\partial k}{\partial x_j}] \tag{28}$$

3.6.3 Two-equations models

The two-equations models are a close system because they can predict properties of a given turbulent flow with no prior knowledge of the turbulence. They are also, the simplest complete model for turbulence [4].

All two-equation models start from the equation (24) knowing that (23). But there are different ways to obtain the dissipation ϵ or the turbulence length scale l. Different models have been proposed, but this study will focus on the RNG k-epsilon model, explained later.

3.6.4 RNG k-epsilon model

The k-epsilon model is the most used one for this cases. The model was developed by Chou (1945), Davidov (1961), Harlow and Nakayama (1972)

and Jones and Launder (1972). The work of Jones and Launder was very important and now its model is called Standard $k-\epsilon$ model. However, the one used in this study is a variation of the latter.

The RANS model used in this study is the RNG (renormalization group) $k-\epsilon$ approach. Renormalization group theory is a statistical method similar to the standard $k-\epsilon$ derivation. This model is an approach from the Navier-Stokes equations that is useful for a wide homogeneous turbulence cases. The model has some refinements that the $k-\epsilon$ model does not include. In epsilon equation there are some new terms that makes the model more accurate for rapidly strained flows. The flow swirls are included in RNG model. It uses an analytical formula for turbulent Prandtl numbers and also accounts for a wide Reynolds number range.

The equation for the dissipation rate ϵ is derived by taking a moment of the Navier-Stokes equation. The amount of algebra needed for this process is not explained in this study for practical reasons. In the article [10] the process is explained.

Then the RNG $k-\epsilon$ model is [11]:

Eddy Viscosity

$$\mu_T = \rho C_\mu k^2/\epsilon \tag{29}$$

Turbulence Kinetic Energy

$$\rho\frac{\partial k}{\partial t} + \rho U_j\frac{\partial k}{\partial x_j} = P_k - \rho\epsilon + \frac{\partial}{\partial x_i}(\alpha_k\mu\frac{\partial k}{\partial x_i}) \tag{30}$$

Dissipation Rate

$$\rho\frac{\partial \epsilon}{\partial t} + \rho U_i\frac{\partial \epsilon}{\partial x_i} = \frac{\partial}{\partial x_i}(\alpha_\epsilon\mu\frac{\partial \epsilon}{\partial x_i}) + C_{\epsilon 1}P_k\frac{\epsilon}{k} - \rho[C_{\epsilon 2} + \frac{C_\mu\rho\eta^3(1-\eta/\eta_0)}{1+\beta\eta^3}]\frac{\epsilon^2}{k} \tag{31}$$

Closure Coefficients

$$\begin{aligned} C_{\epsilon 1} = 1.42, \quad C_{\epsilon 2} = 1.68, \quad C_\mu = 0.0845, \quad \eta_0 = 4.38, \\ \sigma_k = 0.7194, \quad \sigma_\epsilon = 0.7194, \quad \beta = 0.012 \end{aligned} \tag{32}$$

Prandtl number

$$|\frac{\alpha - 1.3929}{\alpha_0 - 1.3929}|^{0.6321}|\frac{\alpha + 2.3929}{\alpha_0 + 2.3929}|^{0.3679} = \frac{\mu}{\mu_{eff}} \tag{33}$$

Where P_k is the turbulent kinetic energy production, $\eta = Sk/\epsilon$ and S the scalar measure of the deformation tensor. To calculate the Prandtl number, $\alpha_k = \alpha_\epsilon = \frac{1}{\sigma_k} = \frac{1}{\sigma_\epsilon}$ and $\alpha_0 = 1$. The parameter β is obtained from experiments.

3.7 Model considerations

Now that the model is chosen some aspects must be taken into account before entering with the implementation. Some parameters must be decided like the Reynolds number, flow velocity, the geometrical parameters. All this will be explained in the following section. As the process to solve the problem is iterative, is very important to chose the correct initial parameters, the k and ϵ. The iterative process and the aspects that affects it will be commented later.

After the theoretical part is done, is very important to see if all the process is done correctly. But is even more important to see if the results of the averaging matches with the equations used in the solver program used, the OpenFoam. After this has been reviewed the study can start.

3.7.1 Wall function

Most two-equations models fail to calculate some parameters near the wall. Applying the no-slip condition and integrating thought the sub-layer will give wrong solutions. This is a problem for wall-bounded control volumes. And in our case, this will be something to take into account. The solution given by the law of the wall needs the parameter B [4].

$$U = u_\tau[\frac{1}{\kappa}\ln\frac{u_\tau y}{\nu} + B] \tag{34}$$

Where $y^+ = u_\tau y/\nu$ is the dimensionless sublayer-scaled distance.

In figure 9 it is easy to see how the law of wall can not approach well the flow velocity near the wall. So a recombination of the wall functions must be performed. They become as follows:

$$k = \frac{u_\tau^2}{\sqrt{\beta*}}, \qquad \epsilon = (\beta*)^{3/4}\frac{k^{3/2}}{\kappa y} \tag{35}$$

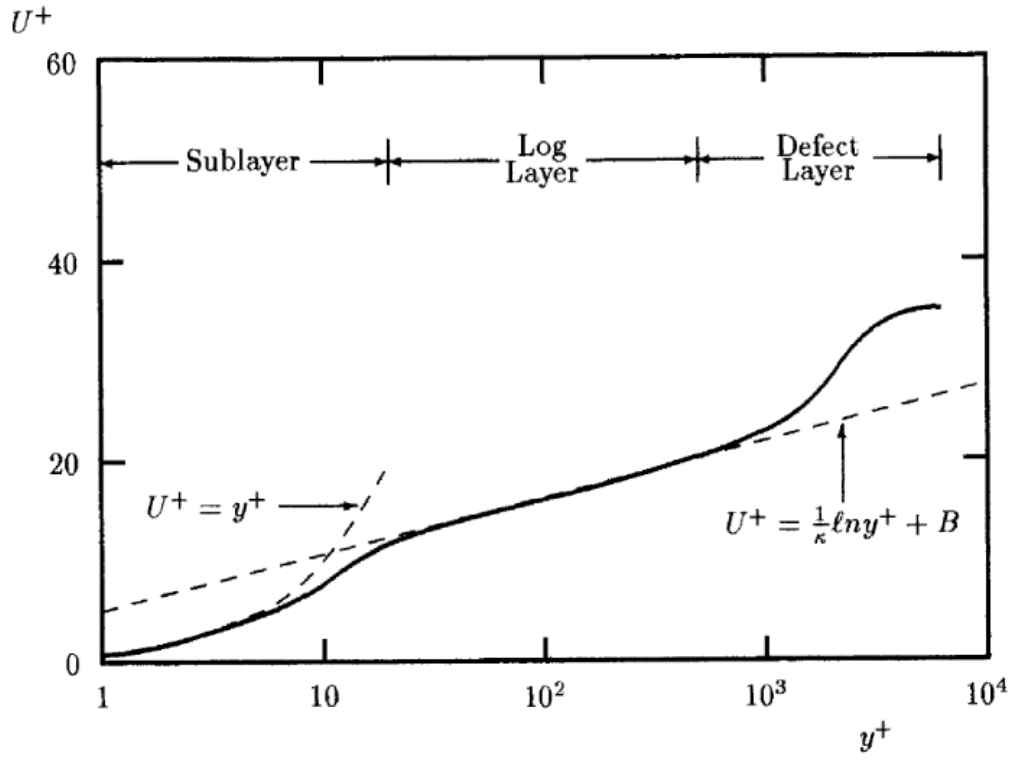

Figure 9: Typical velocity profile for a turbulent boundary layer (extracted from: [4])

For that reason, it will be important to take into account the y^+ value during the simulations.

4 Model validation: two dimensional case

4.1 Description of the case

As it is stated before the RNGk-epsilon model must be validated before solving the main problem of this thesis. Doing this it will be clear that the case of study would be properly solved, with the right equations and approaches. So, some experiments of street canyons will be taken as a reference to validate the model [3]. This means that the CFD study in this section will reproduce the same geometry and flow boundary conditions. By doing that the model should give the solution close to the experimental data. Once this goal is reached, the model is validated. As the turbulence in this case is very low, it is easy to predict that the mean velocity field will be very close to the experimentation data. The fluctuations of the velocity will be the difficult part to validate in this model. As it is mentioned before, the RANS approach model the Reynolds stresses so this means that an error is expected at this part. How the model is applied to this case will be shown later.

The experiment used to validate the model has a total of seven street canyons. The velocity field is measured in the street canyon number four. That is the street canyon in the middle. To validate the model, the solution of the simulation must be taken at the same street canyon. This will be explained later.

4.1.1 Experiment

There is an article from the bibliography where an experiment is done that will be the goal for the model created in this study. The experiment was carry out by Xian-Xiang Li, Dennis Y.C. Leung, Chun-Ho Liu and K.M. Lam in 2007. They study the flow is street canyons of different aspect ratios, 0.5, 1.0 and 2.0. In this case, the aspect ratio is the unit so these are going to be the experimental data of interest. The control volume is a water flume that can maintain a flow rate of $28Ls^{-1}$.

As seen in figure 10, the water is continuously flowing in the circuit thanks to the pump. The geometry of the flume, the control volume, is 10 meters long, 0.3 meters wide and 0.5 meters high. In the following figure 11 a schematic view of the measurement equipment is shown.

The device to obtain the velocity is the LDA, a fiber-optic system. It is a 4-W argon laser that takes the velocity field in the X and Y directions. The

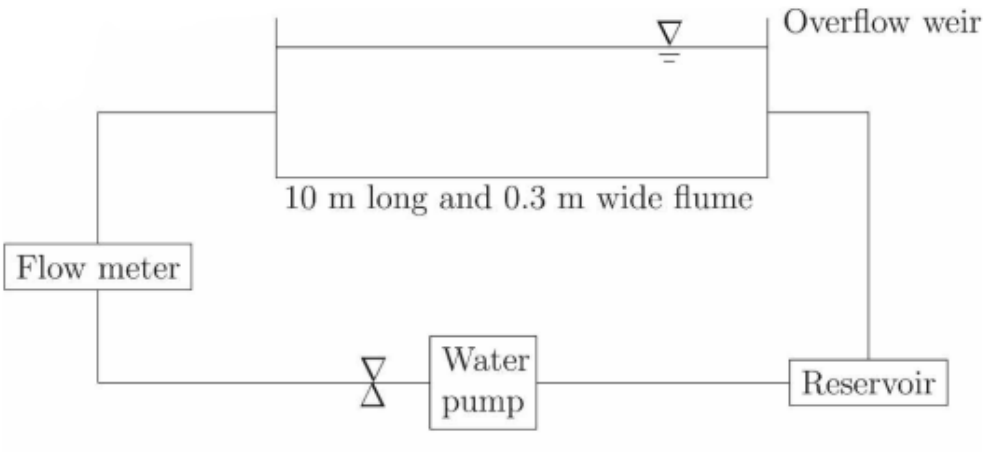

Figure 10: Experimental assembly (extracted from: [3])

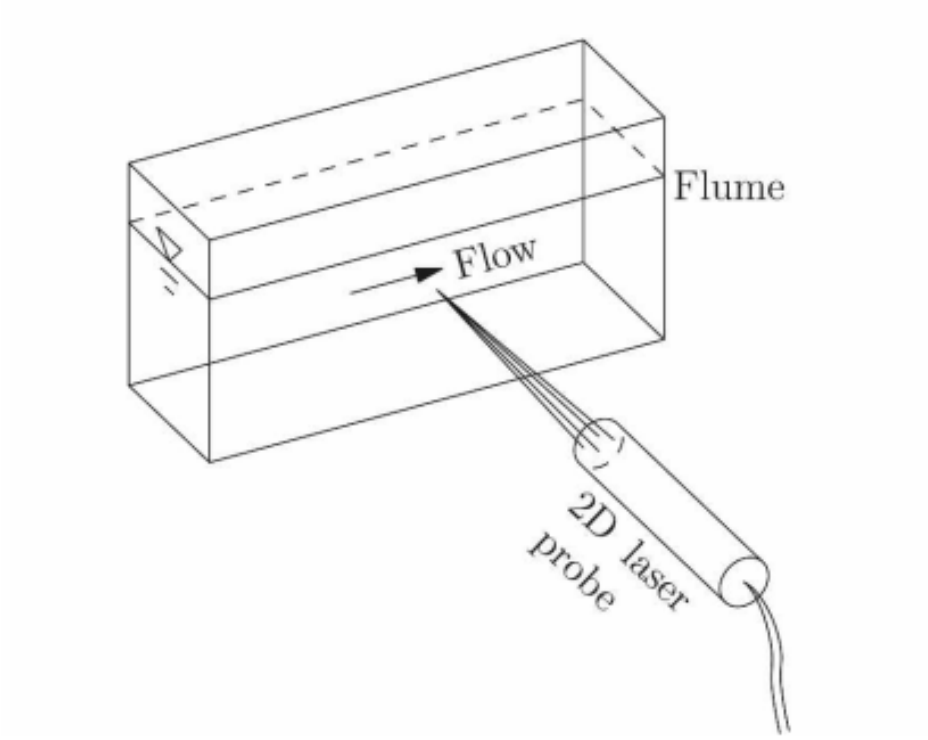

Figure 11: Measuring velocity laser (extracted from: [3])

more interesting thing of this measurement device is that is non intrusive. This means that by measuring the velocity field, it will not be disturbed, in comparison with a pitot tube. As the region of interest is a street canyon

where there is only one way out, the top, it is very important for the flow to not be disturbed.

In the experiment, eight buildings are located in the channel. Those buildings are ten centimeters high, ten centimeters long and have 29.8 centimeters of with so it can fit in the flume. Those buildings have ten centimeters of distance between each other.

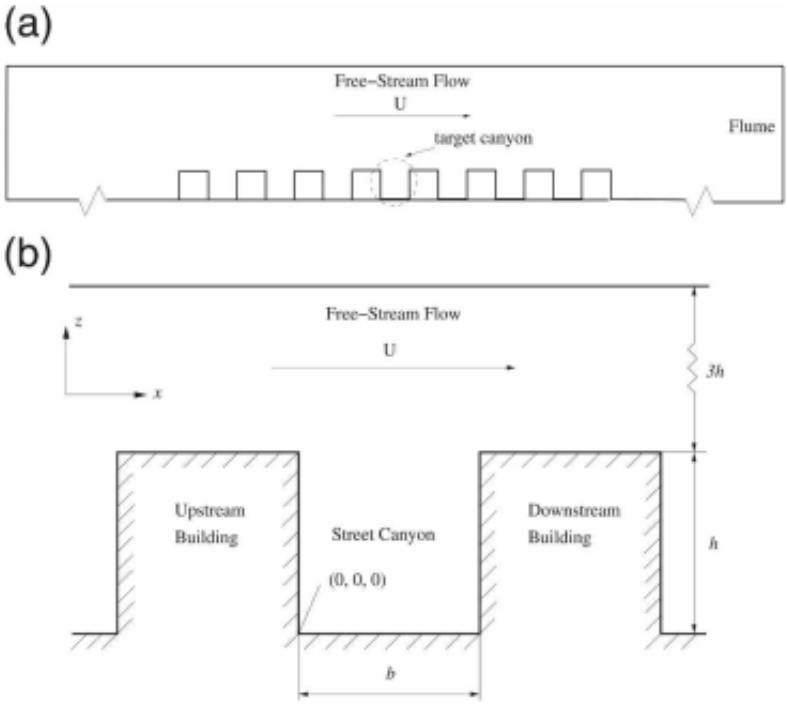

Figure 12: Experiment Geometry (extracted from: [3])

Figure 12 shows the geometry of the experiment, where it shows the axes used in the article. This part is important because the axis in the experiment will not be the same as the ones used in the geometry of the simulation. It has to be clear to avoid any confusion. In the simulation, the X axis will be the one normal to the inlet, the axis that refers to the length of the geometry or buildings. The Y axis will represent the height and the Z is going to show the with of the control volume. This can be easily shown in the Geometry 4.2.

In figure 13, the results of the experiments and simulations for the same case are represented. The dark squares show the results of the experiment. The

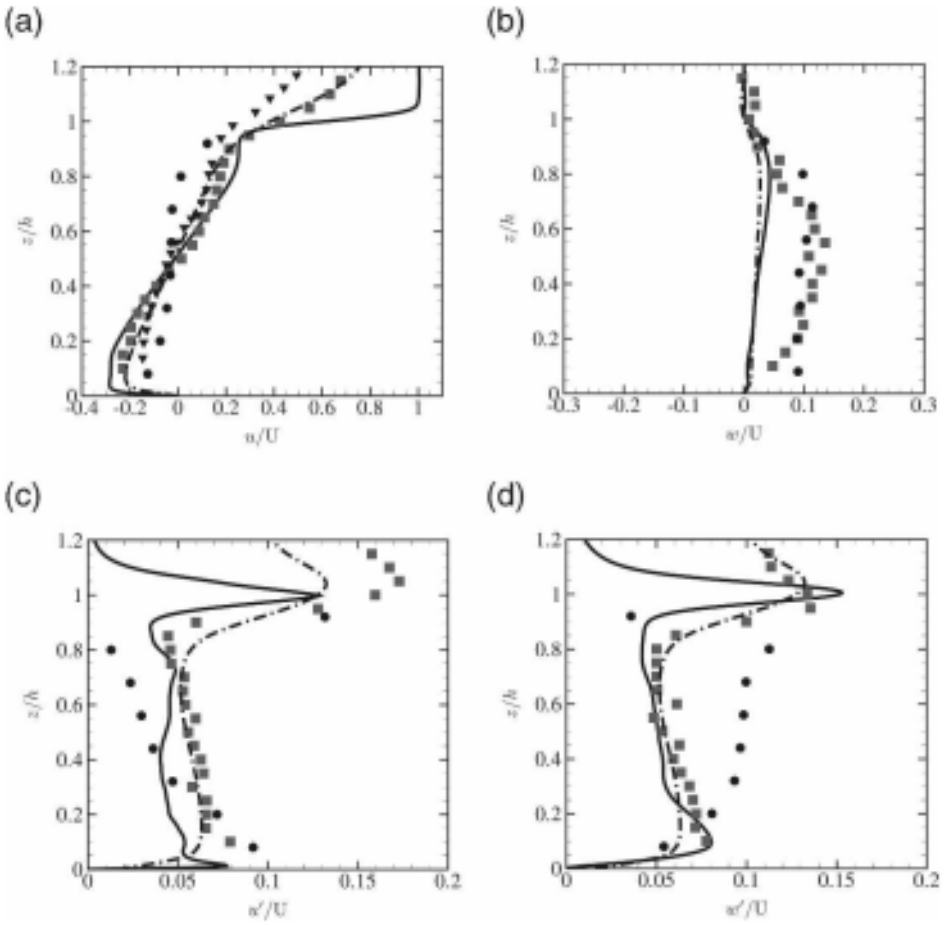

Figure 13: Vertical profile of velocities (extracted from: [3])

straight line is a LES simulation and the dashed-dot line is a $k - \epsilon$ model simulation. The the other ones are different experiments. The inverted triangles represent the experiment for an isolated street canyon and the dark circles for a 7 X 3 array (CEDVAL) [3].

The velocities will be represented as figure 13. In the graphic (a) there are represented the mean velocities in the X direction. In the graphic (b) the mean velocities in the Y direction. And in the graphics (c) and (d) the Reynolds stresses in the X and Y direction respectively. All the velocities and are normalized, that is that they are divided by the freestream flow velocity. This is very important because it makes the results dimensionless. To be able to scale the results to the problem for example, a city, is very important to do that.

A total of five measurements have been done. Three vertical ones from the height zero to 1.2 (as the one in figure 13). Those three have been located in $X = 0.25$, $X = 0.5$ and $X = 0.75$. And two horizontal measurements in the height $Y = 0.5$ and $Y = 1$. In figure 14 it is easy to see the location of the experiments and how have been taken. But in the case of study the axes are not going to be located like this picture. This will be explained later but the axes used in the simulation are X for the longitudinal distances (as the experiments), the Y for the height and the Z axe for the street lenght.

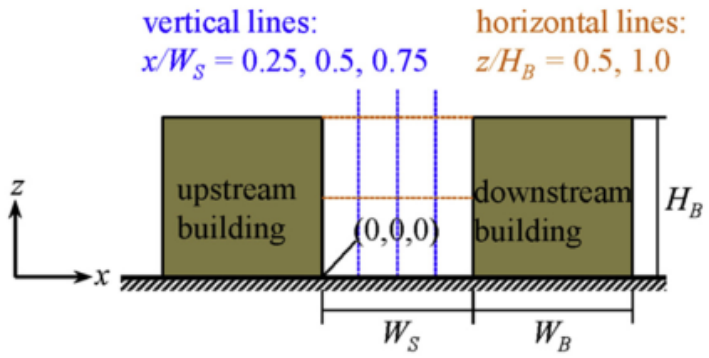

Figure 14: Location of the measurements (Extracted from: [5])

Figure 13 is the only one that will be shown in this study from the experiments [3]. The reason is to optimizing the space, and because the experimental data used to validate the model will be taken and represented later.

This study will focus only in the experiments for the geometry explained, that is the one represented by the dark squares. The other experiments and simulations are not going to be used. The data obtained in figure 13 is a measurement done in the center of the main street canyon.

The fluid used in the experiment was water seeded with polycrystalline powders of nominal diameter at $30\mu m$ to ensure that the laser can measure the flow velocity. The Reynolds calculated in the experiment is $Re = 12.000$.

4.2 Geometry

As it is commented before The street canyon height and length is the unit. There are eight buildings of those dimensions located one unit of distance

one of each other. As the street canyon geometry is a square of the unit at each side, the aspect ration is one $AR = 1$. This will be the aspect ratio used to validate the model. As can be seen in figure 15, having eight buildings make seven street canyons. Then, the street canyon of study will be the one in the middle. Their location are from 12 to 13 meters in the X direction and from 0 to 1 in the Y direction.

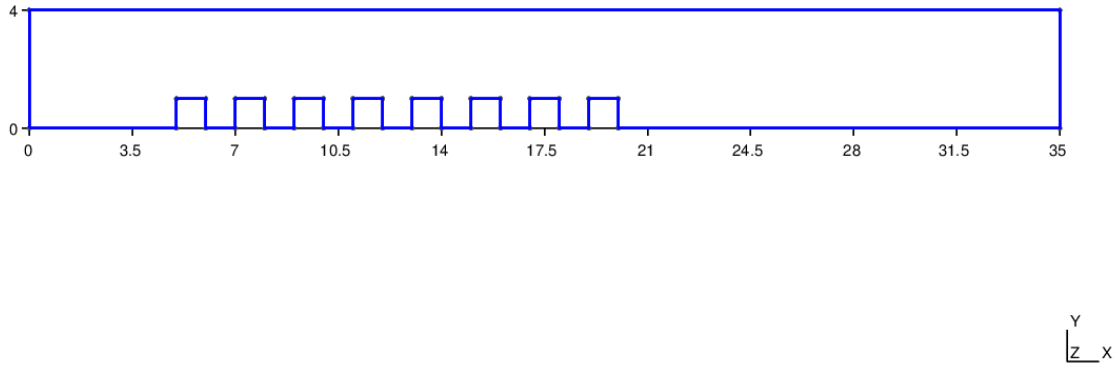

Figure 15: Lateral view of the geometry (generated with: Gmsh)

As the turbulence cannot be solved in a two dimensional case. The solver needs the geometry to have a certain width. The width represented in figure 16 is created with the Gmsh program. Is not a real geometrical parameter, this is built to ensure that the program will solve the problem.

The geometry of the control volume is as shown in figure 16. It height is 4 and the total length is 35. The with has been created by some kind of *extrude* of one *layer* of 3 meters of distance. The distance from the inlet surface and the first building is five meters. This region is needed to see how the flow adapts because of the buildings interference. And the distance between the last building and the outlet region is 15 meters. This is also important to see how the flow recovers its velocity from the interference and to see the wake zone.

To build that geometry in the Gmsh program, the file must be modified as shown in the attachments.

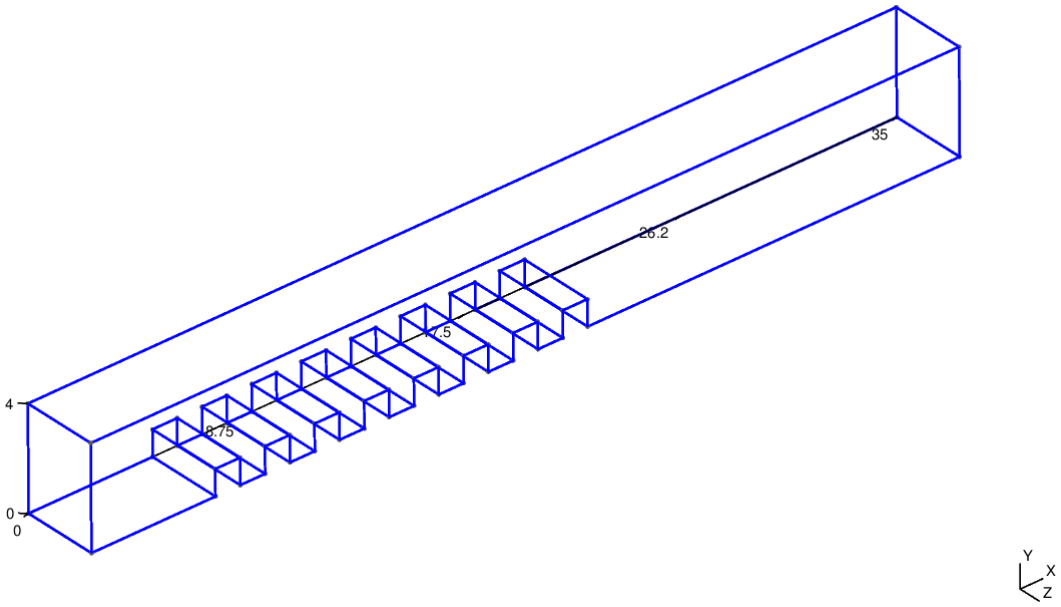

Figure 16: Three dimension view of the geometry (generated with: Gmsh)

4.3 Creation of the mesh

As it is mentioned before, the mesh has been created with the Gmsh open-source program. for the two dimension case, two different meshes have been created. The reason will be explained later. The mesh created for the two and three dimensional cases are unstructured. In figure 17, the mesh created can be observed.

Both meshes have been defined the same way. There are two possible element sizes around a point, $M1$ and $M2$, and it defines how big are they going to be. If it is small, the mesh around it is going to be finer. For computational reasons, the mesh is finer in some regions, and more coarse in others. It is easy to see that the finest region must be the street canyon, and the other ones does not need to be that fine. The points where the element size is $M1$ will be all the points defining the street canyons. And the other points, which are the inlet and outlet points, are defined by the $M2$ element size.

The creation of the mesh is *automatic* by the program, the only parameters that will be modified are the element size explained before [7]. The parameter that is important while creating the mesh is the y^+. This will change in function of the mesh size around the walls. So if the mesh is very

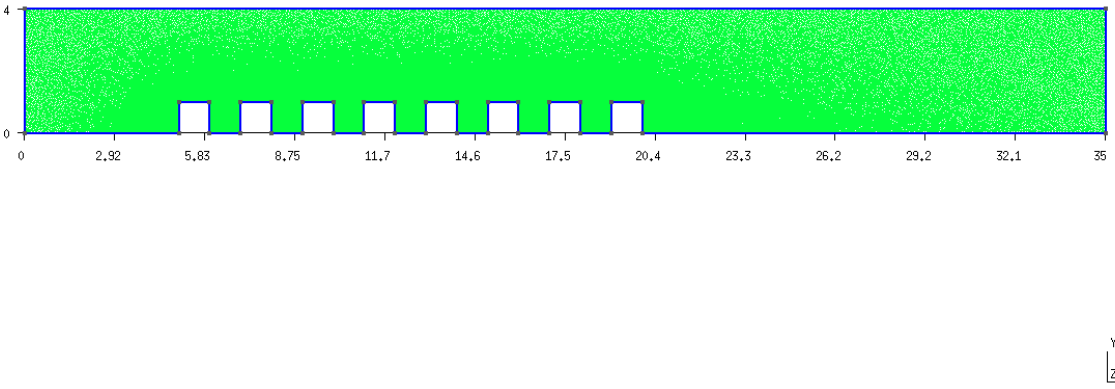

Figure 17: View of the fine mesh (generated with: Gmsh)

fine or very coarse the model will not be able to predict the velocities. It will be explained later that if the mesh is very fine, the computational power is too high to solve the problem with the resources that are available.

The element size parameter works as follows. If a element size around a point is for example $M = 0.05$, this means that the elements will have a size of 0.05 the unit. For example, the line that joins two points of $M = 0.05$ will be divided into 20 elements.

Once the mesh is created, it must be implemmented to the solver, OpenFoam. To do it the following order must be written in the terminal: *gmshToFoam MESH.msh* being *MESH* the name of the file. To check if the mesh is correctly read by OpenFoam, *checkMesh* must be written in the terminal. Then it will appear the number of points and all the data from the mesh.

4.3.1 Fine mesh

The fine mesh has finer element size around the street canyons in comparison with the coarse one but has the same element size in the inlet and outlet regions. This can be observed in figure 18. The element size of $M1 = 0.025$ and the element size of $M2 = 0.1$.

As the mesh is two-dimensional, the elements will be triangles. At the center of each element, a node is located. The node is the point in the space where the equations are calculated, and the nodes around it will be the ones that will disturb it. The fine mesh has around 120.000 nodes.

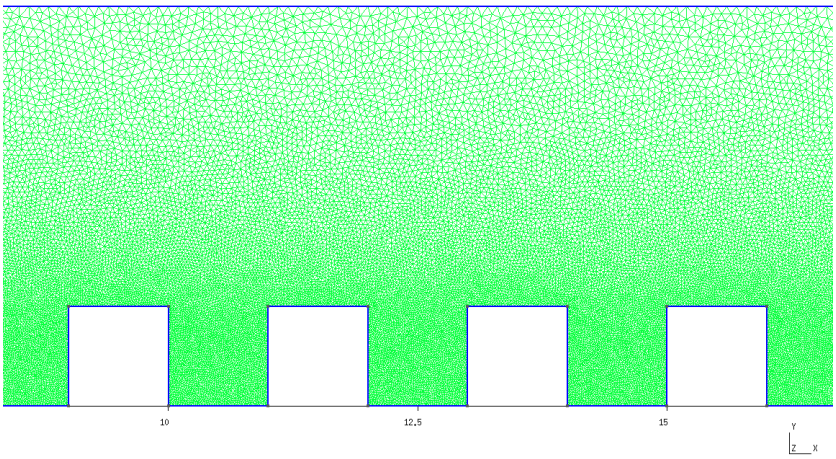

Figure 18: Street canyon view of the fine mesh (generated with: Gmsh)

4.3.2 Coarse mesh

The Coarse mesh has the element size parameters $M1$ and $M2$ located at the same points that the fine mesh. In that case the points at the inlet and outlet surfaces are $M2 = 0.1$. The points of the street canyons have the element size of $M1 = 0.05$.

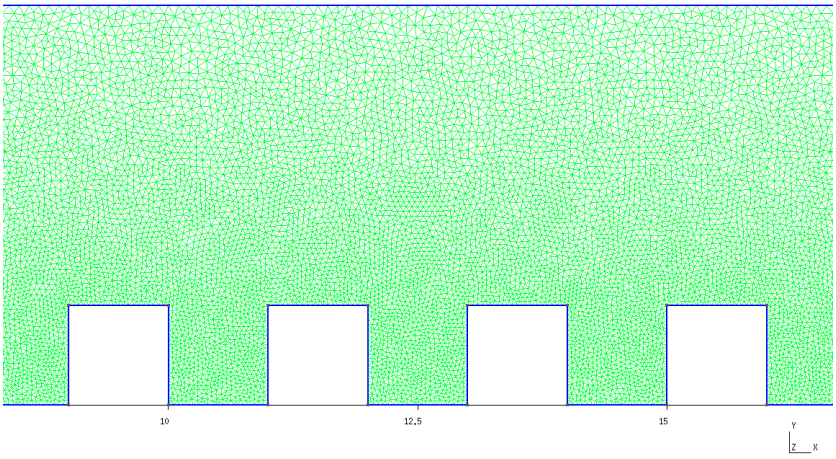

Figure 19: Street canyon view of the coarse mesh (generated with: Gmsh)

In the coarse mesh, there are around 60.000 nodes. So it has half the nodes in comparison with the fine mesh. That does not means that the computing

time in the fine mesh will be two times the coarse mesh. Is very difficult to predict how the time of computing changes, but it could even be more of the double in the fine mesh. The difference can be seen in figure 19.

4.4 Model application

To be able to start with the simulation, the model must be implemented to the solver used, the OpenFoam. This will be told in the section 4.4.2. How the parameters are approached is explained in the section 4.4.1.

As is explained before, some physical parameters must be introduced to close the system of equations. Those are the $k - \epsilon$ values. To refresh what are their meaning, the k is the specific turbulence energy and ϵ is the turbulence dissipation. So to be able to approach those values, there has been created some relations between the physical parameters. From that moment some things must be clear. As those are approaches, the relations taken initially have not worked at first. Some approaches have been corrected by the rule of thumb, it will be notified when. But to obtain the best model to solve the case, a total of twelve simulations have been made. Six of them with the fine mesh and the other six with the coarse mesh explained before. Then, those six have different parameters that modify the k and ϵ values. So six different models have been tested in two different meshes. This will be explained in detail in the following sections.

4.4.1 k epsilon constants

The approaches used to obtain k and ϵ are the following.

$$k = \frac{3}{2}(IU_{ref})^2, \qquad \epsilon = \frac{C_\mu k^{1.5}}{l} \tag{36}$$

Where I is the turbulence intensity and U_{ref} is the free-stream velocity. The turbulence intensity is one of the parameters that will be modified in the different simulations. As the turbulence intensity in the case is low, (no more than the 50%) the values chosen are (0.1, 0.25, 0.5). For the reference velocity U_{ref}, the free-stream velocity is chosen. The free-stream velocity is $U_{ref} = 1.41m/s$.

Once the specific turbulence energy is calculated, the dissipation can be found with the formula (36). Where the parameter $C_\mu = 0.0845$ and has

been rounded to 0.09. Now the turbulence length scale is the last parameter to be found. To do it, the following equation is proposed:

$$l = 0.038 d_h \tag{37}$$

Where d_h is the hydraulic diameter that is calculated with:

$$d_h = 2\frac{ab}{a+b} \tag{38}$$

Where a and b are respectively the height and the width of the control volume. Taking the height and the with of the experiment [3], the turbulence length is $l_1 = 0.013$. This is the first length to be used. The other length taken is the same but divided by ten, $l_2 = 0.0013$. This is done this way because the hydraulic diameter of a street canyon is more or less one tenth part of the hydraulic diameter of the control volume in the experiment. The important part is to have six different values of k and ϵ to simulate six different models.

The k and ϵ values of each model are defined in the table 1.

Case N°	k	ϵ
1	0.03	0.036
2	0.19	0.557
3	0.746	4.46
4	0.03	0.36
5	0.19	5.57
6	0.746	44.56

Table 1: Different models simulated

So as the different models have been simulated with different meshes, the twelve simulations are explained in the table 2.

Simulation table				
	Coarse Mesh		Fine Mesh	
	$l = 0.013$	$l = 0.0013$	$l = 0.013$	$l = 0.0013$
$I = 0.1$	Model 1	Model 4	Model 1	Model 4
$I = 0.25$	Model 2	Model 5	Model 2	Model 5
$I = 0.5$	Model 3	Model 6	Model 3	Model 6

Table 2: Models' distribution

4.4.2 Implementation in OpenFoam

To be able to solve the simulation with OpenFoam, the *pisoFoam* model is used. This means that in the main directory, the 0, the *constant* and the *system* directories are going to be placed. In that directory, the mesh must also be placed. To impose the conditions to the geometry, each surface must be defined previously. There are the inlet and outlet surfaces, where the flow enters and leaves the control volume, respectively. The top surface and the wall surface. And finally, the left and right surfaces.

In the 0 file the initial conditions must be applied. So the most important files to modify are going to be the k, ϵ, U, and P. In this case, the geometry is two dimensional, so the left and right surfaces will have the empty condition for those files. This was explained before, the two dimension geometry needs a extruded surface to be able to calculate the turbulence.
In the pressure file, it needs the fixed value in the outlet of 0. This is to ensure that the flow leaves this surface without collapsing the control volume. The other surfaces have the *zeroGradient* condition to ensure that the pressure does not suffer any change through those surfaces.
In the velocity file, the inlet has the fixed value of $(1, 0, 0)$. Then, the slip condition is imposed in the top surface to ensure that the flow does not *leave* from this surface. It is also imposed because that surface can not slow down the flow. And in the wall, the no-slip condition ensures that the flow velocity in the wall is $(0, 0, 0)$.
The k and ϵ files are very similar one to each other. Both have the empty condition at the right and left surfaces. An internal field of the value chosen is needed. Then, the wall-function must be applied in the wall surface. The inlet needs the fixed value of the parameter and finally all the other surfaces will have the *zeroGradient condition*.
There are also the *nut* and *nuTilda* files with an internal field of zero.

In the *constant* directory, a lot of files related with the geometry are cre-

ated when the mesh is imported. There are also the *transportProperties* and *turbulenceProperties*. In the first one, the kinematic viscosity is $\nu = 0.000083$. This is obtained from the Reynolds equation:

$$Re = \frac{LU}{\nu} \tag{39}$$

Where the velocity and the characteristic length are one, the Reynolds is 12.000. This number is chosen because is the same Reynolds number used in he experiment [3].
And in the *turbulenceProperties* file, the Reynolds-averaged Navier-Stokes model used must be specified, in this case, *RNGkEpsilon*.

And finally, in the *system* directory there are three files, *controlDict*, *fvSchemes* and *fvSolution*. Where the last two contains the solver used, and the methods to find the solution. The first one has the time that the simulation should start and the time that should end in seconds. It also has the increment of time that is going to be used. This will decide how many iterations the solver is going to use.

4.5 Results

In this section, the results of the simulations are going to be presented. The discussion will be done later. The comparison between the experimental results and the simulations are going to be shown. The streamlines of the flow are also going to be presented.

4.5.1 Convergence

Once the program has done the simulation, is very important to see if the solution has converged or not. As the mathematical solution of the program is iterative, the error (or residual) that appears calculating the pressure and the velocities must be studied. And it has to approximate to zero while the simulation is running. But it must stand stable at some value. When this happens, the transition zone is exceeded. Then, in the *stationary* zone, the residuals must fluctuate around a value.

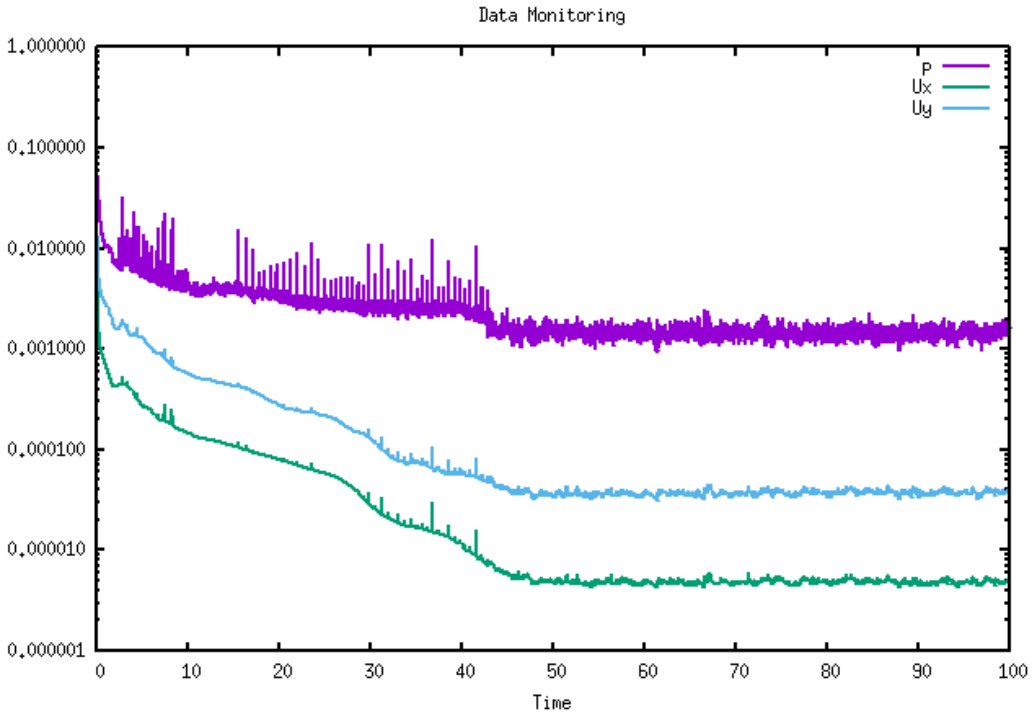

Figure 20: Residuals evolution in a two-dimension simulation

Figure 20 shows an example of how the residuals has developed during a simulation. It is very easy to see that around the second 45 the transition zone has been exceeded. From that moment, the solution has converged.

Simulation table				
	Coarse Mesh		Fine Mesh	
	$l = 0.013$	$l = 0.0013$	$l = 0.013$	$l = 0.0013$
$I = 0.1$	Converged	Converged	Converged	Less Converged
$I = 0.25$	Converged	Converged	Not Converged	Converged
$I = 0.5$	Not Converged	Not Converged	Not Converged	Not Converged

Table 3: Convergence of the models

The table 3 shows how the twelve simulations have converged.

4.5.2 Velocity map

Before the comparison between the experimental results and the simulations, the velocity maps of the simulations are going to be shown in figures 21 and 22.

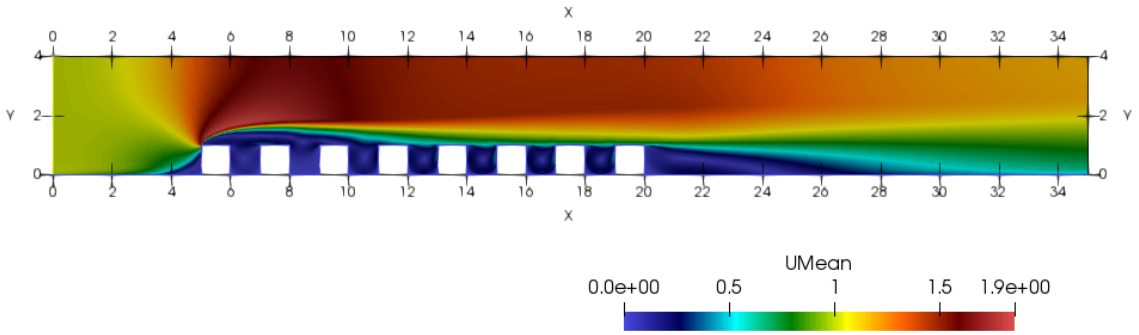

Figure 21: Velocity map of the two dimensional case

Figure 21 is the velocity map of the model 5 in the fine mesh. This is the model that has the best approach to the experiments. Now, how the flow is affected by the geometry of the buildings is going to be discussed. Figure 22 has a more detailed view.

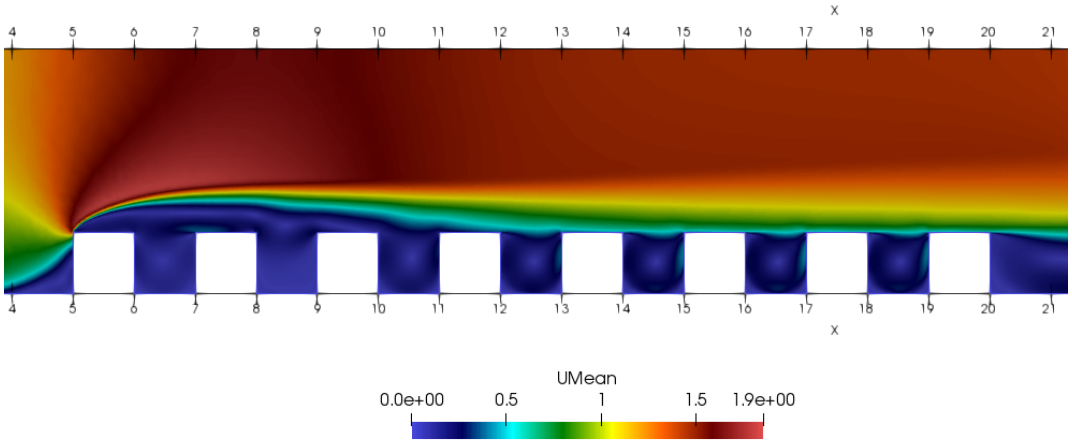

Figure 22: Velocity map in the street canyons

In figure 22 is easy to observe that the suction zone of the first building affects the following three street canyons. Until the fourth street, the eddy is not stable. This is the reason why the experiments and the simulations have been done in this canyon. The following streets to the right have an eddy with the same shape, so they have the same velocity map.

To be able to see what has been explained before, a map of the velocity streamlines has been done. It can be observed in figure 23.

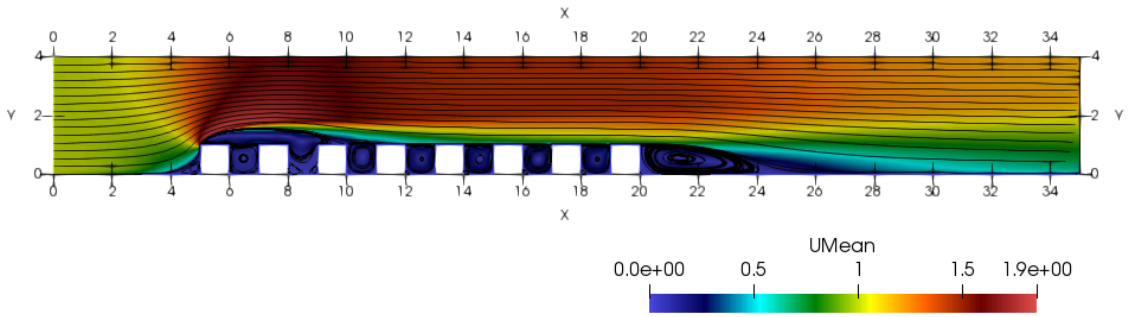

Figure 23: Velocity map in the street canyons

Now with the velocity streamlines, it is easy to observe that the four regions generated by the disturbance of the flow have been simulated very well. The zone where the air is still not disturbed and the zone where is displaced is recognized. All the places where the flow has a low velocity, colored with blue, are the suction zone. And is easy to see the zone where the flow is recovering its state, the wake zone.

And finally, the street canyon of study, the one in the middle, has an eddy that will be studied. The velocity streamlines of each simulation will not be presented, but a comparison between two of them will be made. As the velocity map shown before, the model chosen is the number five.

In figure 24 the simulation shown is the coarse mesh with the model five. It can be seen that the eddy has been well simulated. In figure 25, there is the same view of the street canyon. In this case, is the same model (number five) but simulated with the fine mesh.

In this simulation, the eddy has also been well simulated. But making a comparison between them there is an important thing to talk about. Quali-

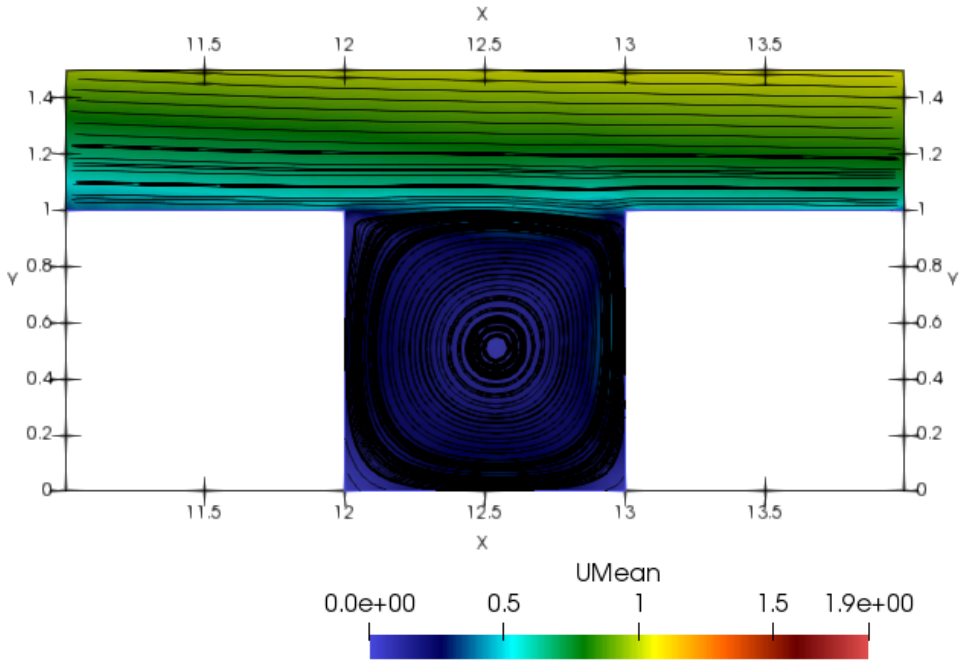

Figure 24: Street canyon of study. Detailed view of the velocity streamlines. Model 5, coarse mesh

tatively the same model has simulated well the velocity with the two meshes. But paying attention on figures, it can be seen that the fine mesh has been able to simulate an eddy on each corner. Clearly, this is because of the mesh size. If the elements are bigger, the eddy on the street canyon is going to be simulated well, but the details will not be captured. Other details, like the corner in the top of the left building have been simulated much better in the fine mesh.

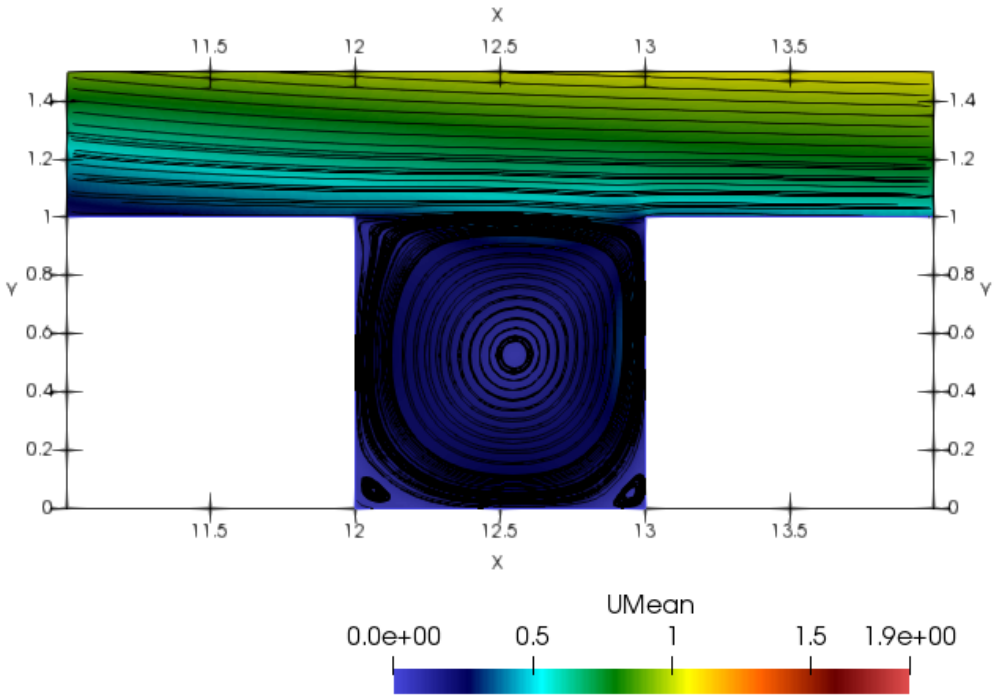

Figure 25: Street canyon of study. Detailed view of the velocity streamlines. Model 5, fine mesh

4.5.3 Simulation results

Now, a comparison between all the simulations and the experimental results is going to be show. Later, a discussion will be done. Five figures are presented, one for each measurement in the experiment [3]. As it is explained before, each one has the mean velocity and the fluctuations in the X and Y directions.

Each figure will show the following lines: The black circles represents the data taken from the experiment. Then, there are the lines from the simulation. The dashed lines show the simulations done with the coarse mesh, and the straight lines represent the simulations done with the fine mesh. To identify the different models in figures, each one has a colour. The model one has the black, the two has the green, the colour red for the fourth model and the colour blue to represent the model number five. The table 4 shows the legend used in figures comparing the experiments and the simulations (26, 27, 28, 29 and 30).

Key table				
	Coarse Mesh: dashed line		Fine Mesh: straight line	
	$l = 0.013$	$l = 0.0013$	$l = 0.013$	$l = 0.0013$
$I = 0.1$	Black	Red	Black	Red
$I = 0.25$	Green	Blue	–	Blue
$I = 0.5$	–	–	–	–

Table 4: Key of figures

In figure 26, 27, 28, 29 and 30 and as has been explained before, W_s is the length of the street and H_b is the height of the building.

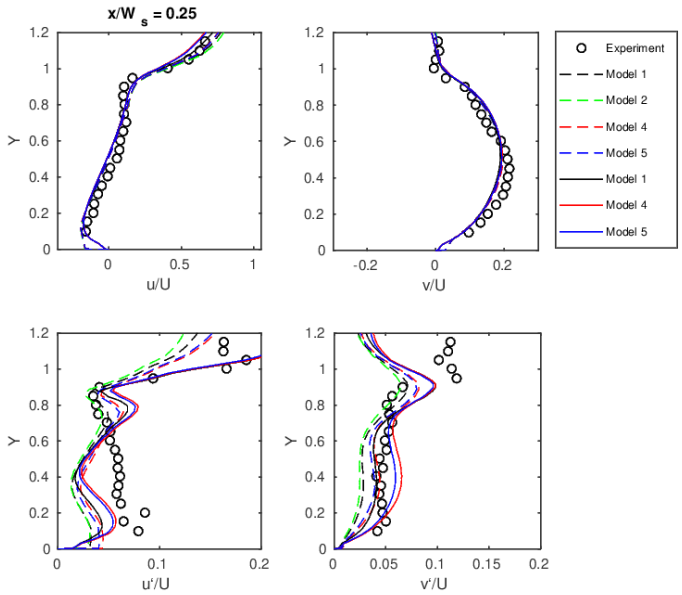

Figure 26: $RNGk - \epsilon$ models comparison with experiments at $X = 12.25$

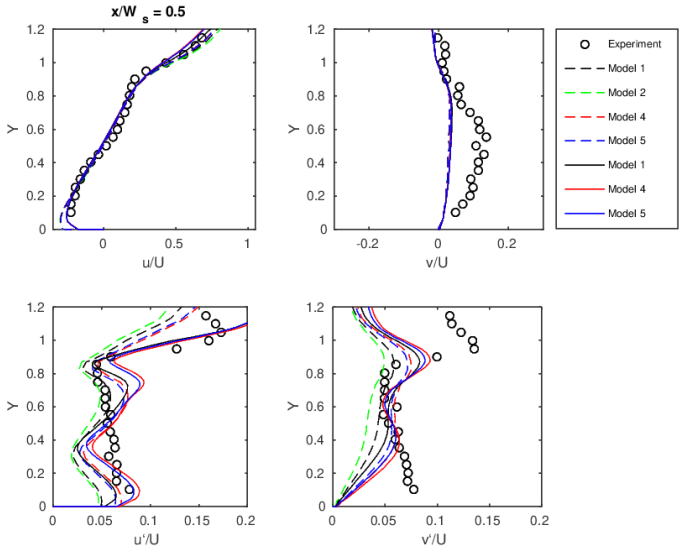

Figure 27: $RNGk - \epsilon$ models comparison with experiments at $X = 12.5$

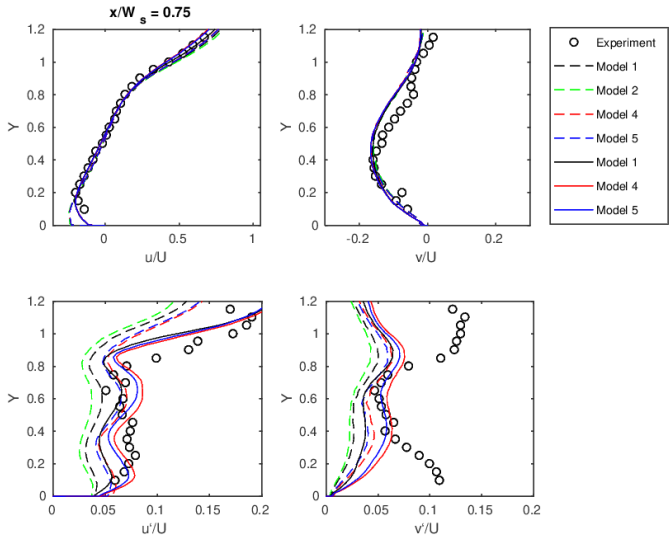

Figure 28: $RNGk - \epsilon$ models comparison with experiments at $X = 12.75$

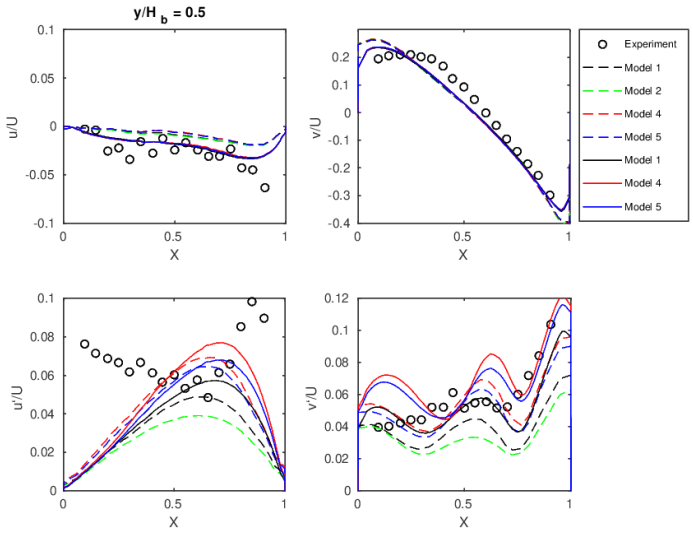

Figure 29: $RNGk - \epsilon$ models comparison with experiments at $Y = 0.5$

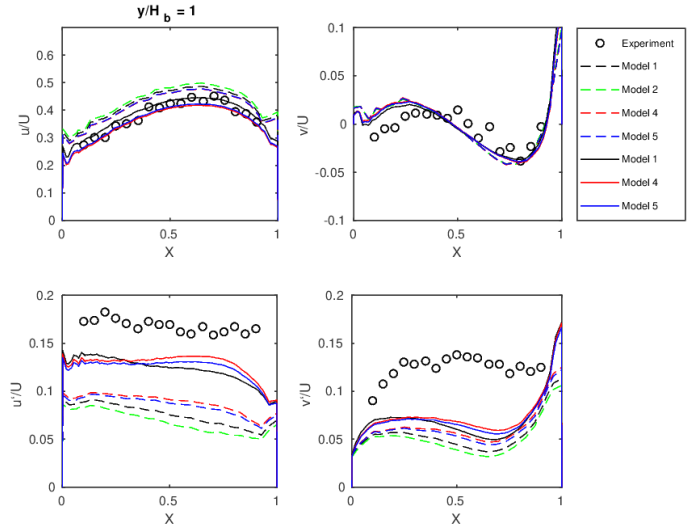

Figure 30: $RNGk - \epsilon$ models comparison with experiments at $Y = 1$

The seven simulations that have converged are the ones taken to compare with the results. To process the data, obtain the velocities and making the color-maps, the Paraview program is used. And to build the graphs, give the color and the shape, the MatLab is used.

4.6 Discussion

Now that all the results have been presented, a conclusion on the validation of the model can be made. If the model is validated, the first part of the project is reached,as well as the rest of the objectives proposed in the first part Now, there is enough information to see if this is completed.

After the twelve simulations, just seven have converged. Those are the ones studied. From the graphics the following conclusions are obtained.

4.6.1 Mean velocity

The first thing that can be seen is that all models can simulate the mean velocities with precision. Just when $Y = 1$ (in figure 30) and $Y = 0.5$ (figure 29) there are some differences depending on the mesh used. This is a very good sign because it means that the $RNGk - \epsilon$ model is a good model for those cases. Talking about a flow simulation, the mean velocity and the fluctuations are both important, but the mean velocity gives the general state of the flow, and if the model is capable of simulating it, this will mean that is a good model. Nevertheless, so as to validate it, it has to be able to simulate all the state of the flow, the mean velocity and the fluctuations.

There is one situation where the model has a small error. This appears in figure 27 where the mean velocity in the Y direction of all the simulations have a different path than the experiments. This error could appear because of a bad measurement in the experiments.

4.6.2 Reynolds stresses

From a general point of view, the models that uses the fine mesh, are the ones that can approach the Reynolds stresses better. In some cases this is very clear, for example in figure 30.

It is seen from the results, that the Reynolds stresses are well simulated in general. In some cases, the shape is more exaggerated. And in others, the simulations follow well the path of the experiments.

A phenomena observed is that the flow velocity in the normal direction near the wall is very hard to predict. This is seen in figures 30 and 29, which have some errors close to the $X = 0$ and $X = 1$ position. In figures 26, 27 and 28 this phenomena is also found. Comparing the results next to the $Y = 0$ position, the fluctuations in the X direction are better simulated than the ones in the Y direction.

The model has some small errors simulating the fluctuations normal to the eddy in the exterior zone of it. This could appear because of the interference of the wall if the wall-function has some errors, for example. Or it could be that the experiment has some errors in measuring the exterior zones of the eddies.

In conclusion, the fluctuations of the velocity are the most difficult part to model, so the error was expected because of the precision of the (RANS) model. It could be stated that this is the reason why the fluctuations are well simulated but with small errors in some points.

4.6.3 Validation of the model

Now, the best model to approach the flow state must be chosen.

As it is explained before, the models using the fine mesh have a better approach to the solution. But when paying attention to model number one simulated with the fine mesh (straight line in black), it can be seen that even the models four and five with a coarse mesh have better approaches. Some graphs show that those two models are better than the number one and in some others that the solution is more or less the same. This appears in all the cases except in figure 30.

Therefore, when trying to determine the best models, it is very clear that numbers four and five are the best ones simulated with the fine mesh. Those two show always the same results and more or less with the same precision. But looking at the convergence table 3, model four with the fine mesh is not well converged. Then, the model taken will be number five. Looking at this table again, it can be stated that the simulations are harder to converge for finer meshes. This was something expected because the increment of time must be more precise. It will cost more computational time to simulate it.

Taking all that has been stated before, the model is validated. Now, the

last requirement of the first part is completed.

The following part of the project will be making a three dimension simulation with the model chosen before, the number five where $k = 0.19$ and $\epsilon = 5.57$.

5 CFD study: three dimensional case

5.1 Description of the case

In the three dimension simulations, the model is already chosen. This means that the constants to approach the solution are going to be $k = 0.19$ and $\epsilon = 5.57$. With this geometry, the main problem will be solving the case with a converged simulation. It is expected that the problem will take a lot of computational power. For that reason, the simulations of the three dimensional case are solved with the director's computer.

Now, the main objective of solving the problem is to see how the flow in the street canyon changes when changing the aspect ratio $AR = \frac{H}{W}$. The dispersion of air will be compared with different street geometries. The aspect ratios chosen are from one to two, and all possible cases between them. The amount of cases that have been solved will be commented later.

5.1.1 Geometry

Now that the geometry is three dimensional, it must be created from zero. In this case, the most difficult part in the process of creating the geometry has been the huge amount of points and lines. In the attachments, its complexity can be seen. In figure 31 the geometric parameters are shown.

It can be noted that the geometry is the same in the X and Y directions, but the buildings have a width of 3, and the distance between the buildings and the end of the control volume is 1.5 at each side. The rest of the geometric parameters have been already explained.

In figure 32, the geometry of the $AR = 1.25$ case can be visualized. Now, the only difference is that the street width is 0.8. There will not be figures of the geometry of the different aspect ratios to optimize the space.

5.1.2 Creation of the mesh

Now that the control volume is three dimensional, the mesh will suppose a big problem. If the mesh is fine, the computational power needed will be very high. And if the mesh is coarse, the simulation will not be able to solve the problem or maybe it will not converge.

In figure 33 the geometry can be seen from an another point of view. From this perspective it can be seen how the mesh fills the control volume.

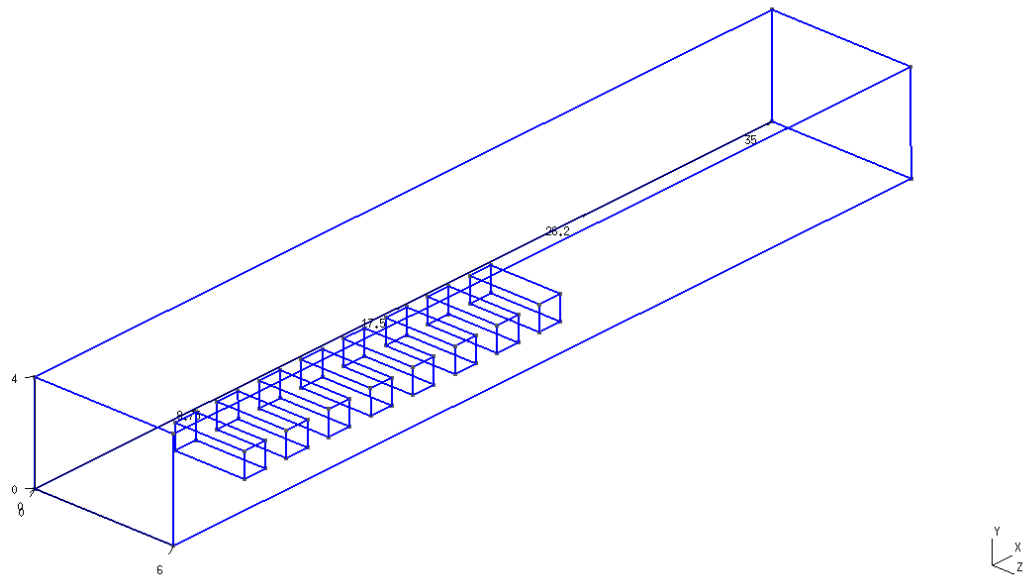

Figure 31: Three dimension geometry (generated with: Gmsh)

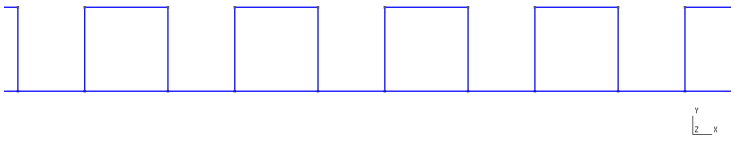

Figure 32: Geometry of the AR = 1.25 (generated with: Gmsh)

The element size chosen in this case is different from the two dimensional. As it is said before, the mesh can not be so fine for computational power reasons. Now the element size will be $M1 = 0.1$ and $M2 = 0.3$. And also the distribution of the points have changed. In this mesh almost all the points will have the element size of $M2$. The points with the smallest element size are the ones around the street canyon of study. The mesh has been created

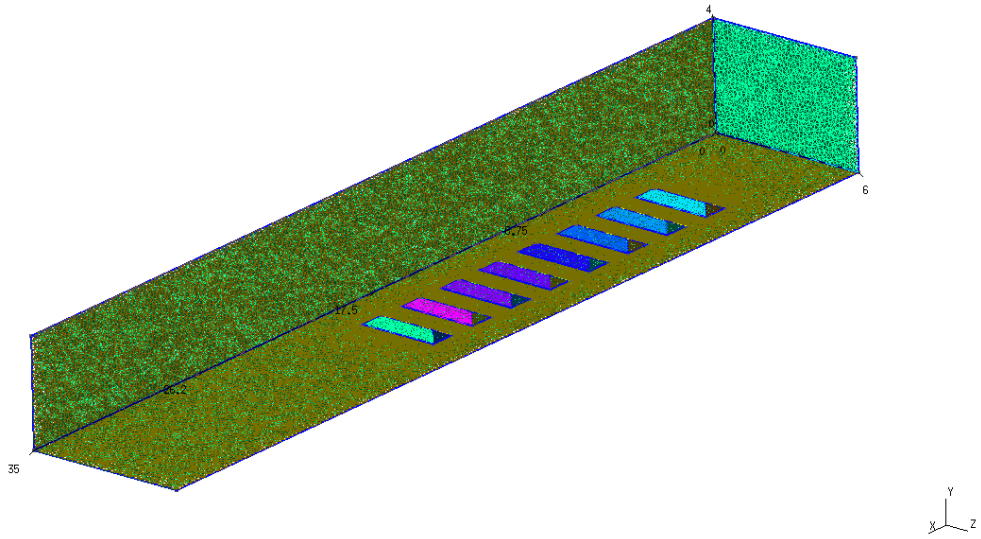

Figure 33: Superficial mesh (generated with: Gmsh)

this way to optimize the computational time knowing that the results will not be very accurate.

In this case, the creation of the mesh is easier that the geometry. The program fills the surfaces and the volume with the unstructured mesh. Some lines to the code must be added to ensure that this is done correctly.

5.2 Model application

In this section, the model is already chosen so the k and ϵ constants will not be calculated again. Now, the main variation in the simulations will be in the mesh and the increment of time. This is because of what has been explained before, it is harder to found the optimum mesh size and increment of time to run the simulations.

5.3 Results

The results of the three dimensional case will be presented. As it has been commented before, some cases will be simulated. Those will have the same characteristics, but the aspect ratio will be changing. In the results the velocity maps and the velocity graphs will be presented as it is done in

the two dimensional case. Later in the discussion, the results of the three dimensional case and the two dimensional case and the two simulations with different aspect ratios will be studied.

5.3.1 Convergence

As expected, convergence has been the main problem. From a qualitatively point of view, the solution has not converged. But as this was expected, some simulations have been taken as good ones even though they have not fully converged.

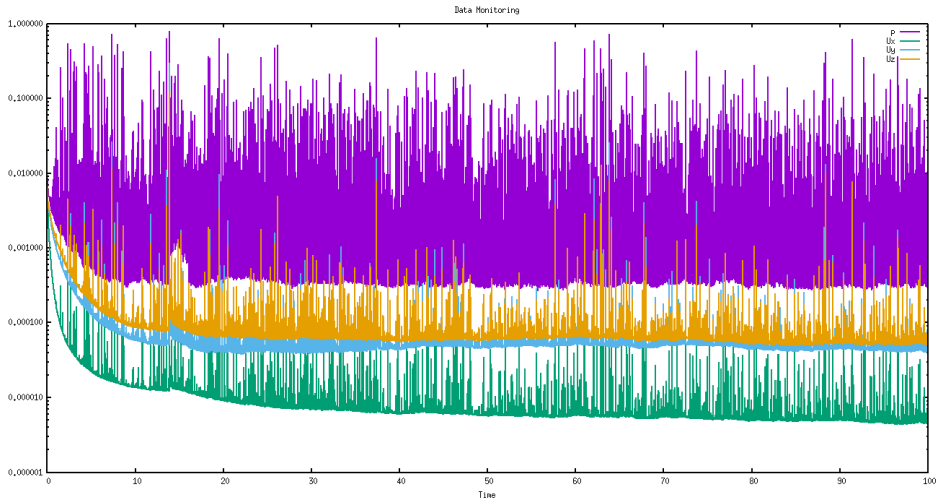

Figure 34: Convergence of a three dimensional case

As can be seen in figure 34, the velocities will have an error around 0.00001. But as the solution has not gone to a very stable point, it is hard to say if this has completely converged.

5.3.2 Velocity map when AR = 1

As in the two dimension simulation, the velocity map and the streamlines will be shown. In this case, as the control volume is three dimensional the figures will be different. There will be a qualitative comparison between the two simulations.

The case where the aspect ratio is $AR = 1$ will be presented first.

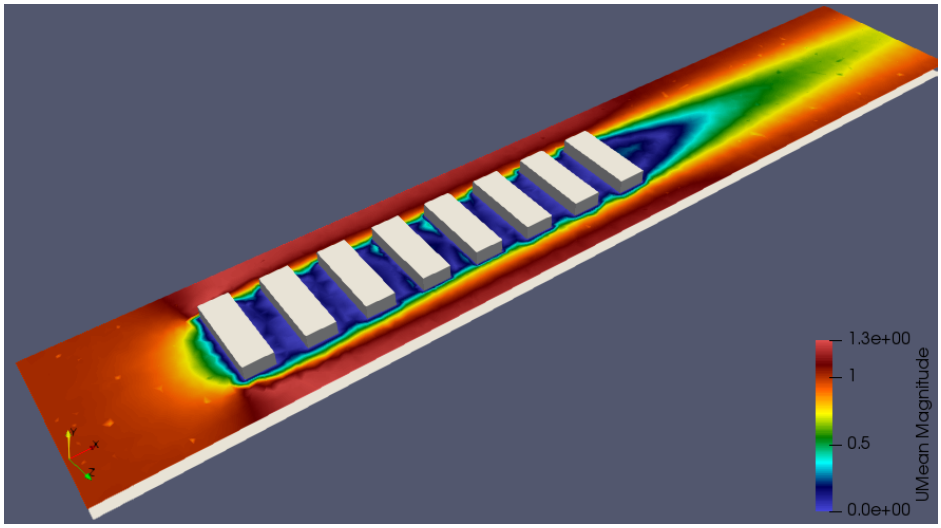

Figure 35: Velocity map at Y = 0.5, (Y normal) when AR = 1

In figure 35, it is easy to see the behaviour of the flow when the control volume is three dimensional. At each side, the velocity increases as it did before with the flow over the buildings. It is also very easy to observe the heat island effect. As the velocity between the buildings is lower it decreases the air dispersion.

And in figures 36, 37 and 38, a lateral view of the velocity map will be presented is some point of the volume. There, it will be easy to observe that the canyon number four is better simulated, this is because the mesh is finer there as has been explained before.

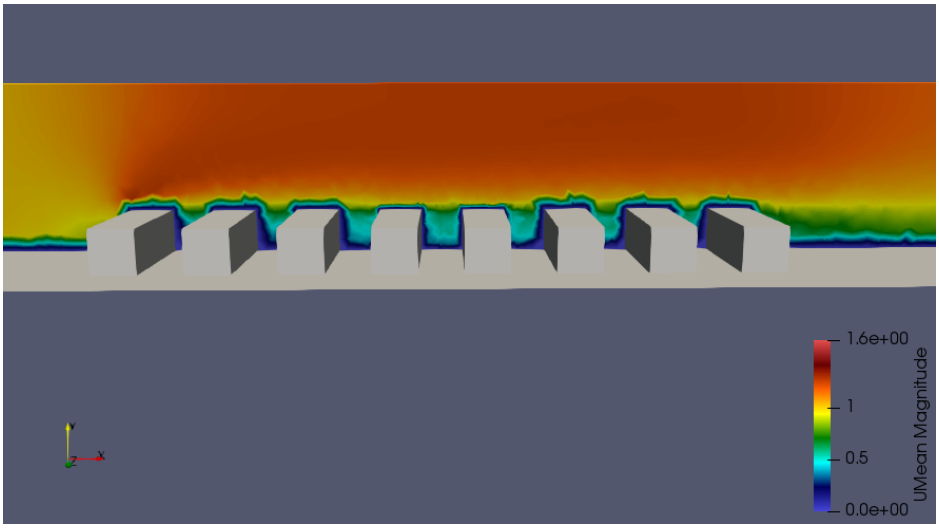

Figure 36: Velocity map at Z = 1.5 (Z normal) when AR = 1

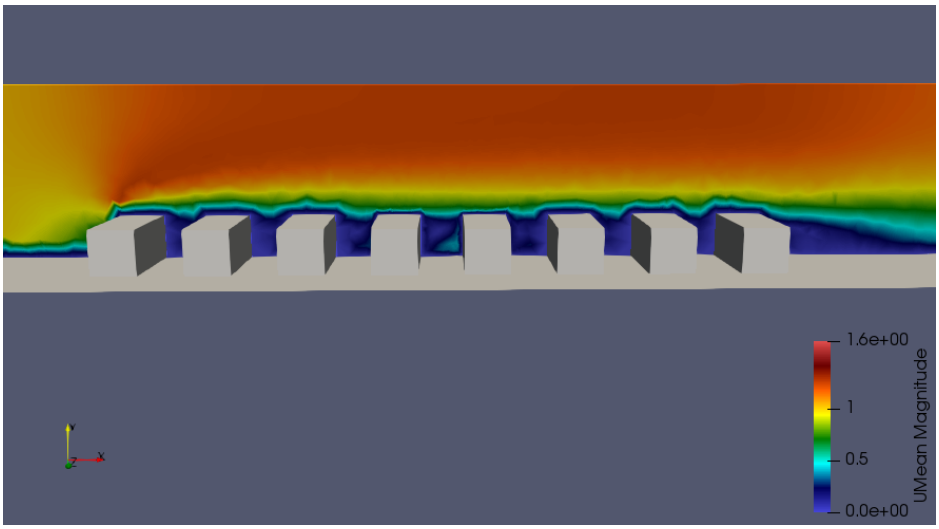

Figure 37: Velocity map at Z = 2.25 (Z normal) when AR = 1

Figures 36, 37 and 38 are located the following way. The position of the first one is just at the beginning of the street and the last one in the middle. The second one is located between them to be able to see the evolution. So those three figures present how the flow develops when it is closer to the middle of the street canyon. The flow in the middle of the control volume $Z = 3$, has the most similar velocity field comparing to the two dimensional one. It also can be seen that when the flow approaches to the middle, it decreases its velocity.

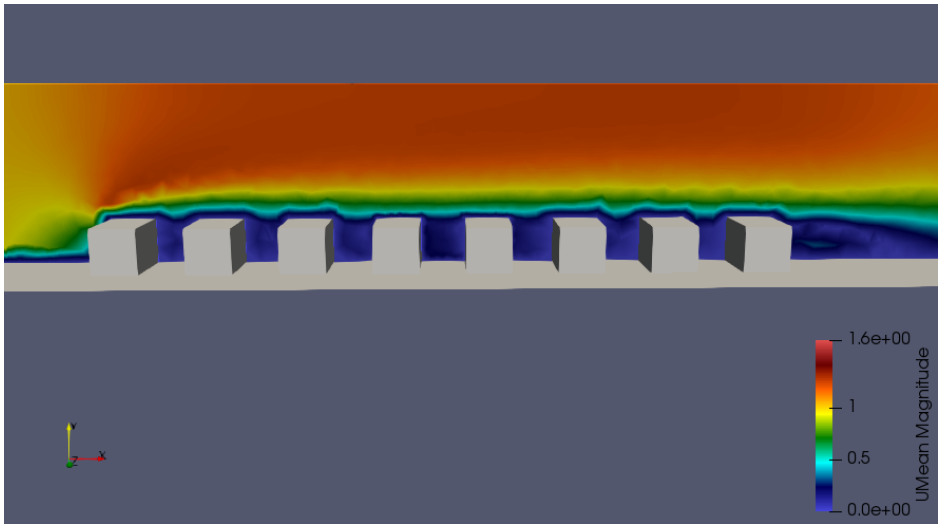

Figure 38: Velocity map at Z = 3 (Z normal) when AR = 1

The streamlines of the three dimensional case over the buildings are shown in figure 39.

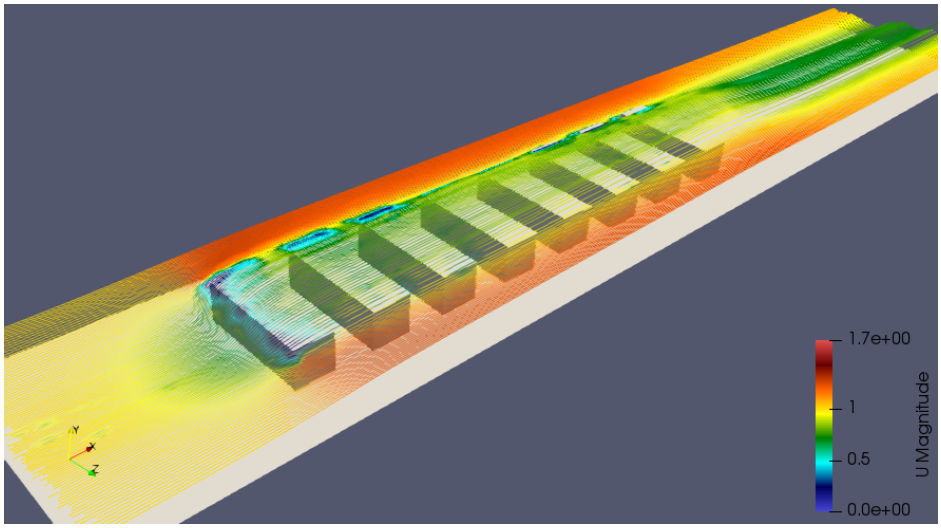

Figure 39: General view of the streamlines in the three dimensional case when AR = 1

Now, some figures are going to be presented in order to visualize how the streamlines behaves in the street canyon of study.

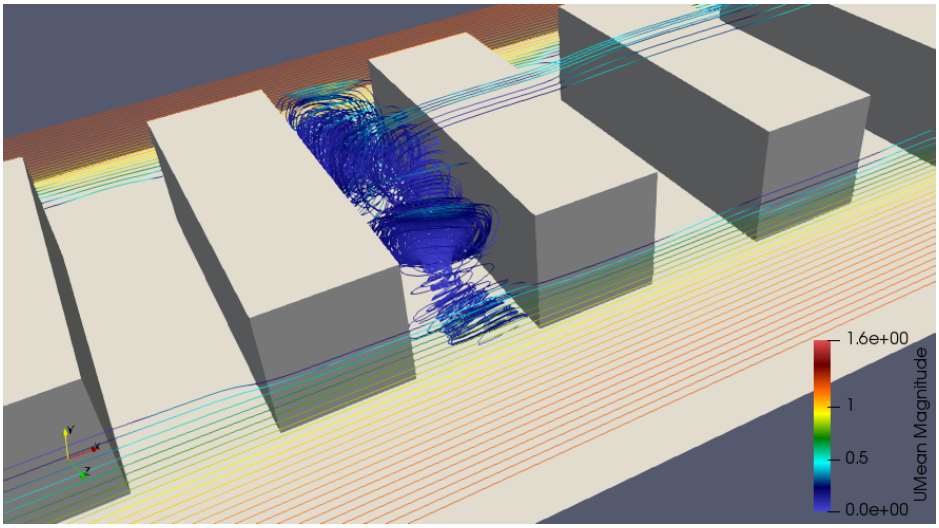

Figure 40: Turbulence inside the street canyon of study when AR = 1

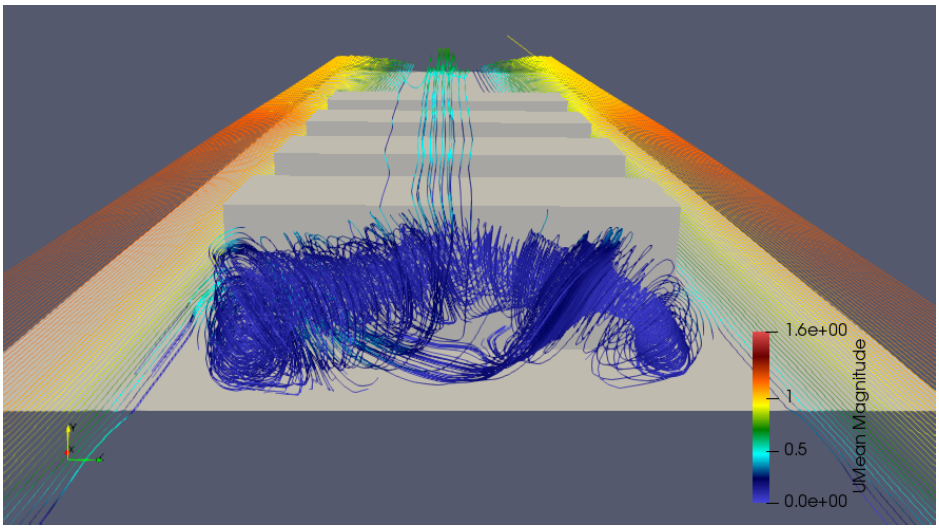

Figure 41: Frontal view of the eddies inside the street canyon when AR = 1

Figures 40 and 41 are very interesting. It can be easily observed how the flow develops inside the street canyon. What those figures present are the mixing of two eddies. First, the one observed before in the two dimensional case. An secondly, the two eddies that enters to the street from the sideways. This makes that the three dimensional eddy created has the shape of a *bridge*. It can be seen in figure 41 that it looks like an inverted *U*.

What can be deduced from figures 40 and 41 is that the flow is very well

simulated even in that complicated case. This will be commented later.

5.3.3 Velocity map when AR = 2

And now, the velocity maps of the three dimensional case with $AR = 2$ are going to be presented. The velocity maps can be seen in figures 42 and 43.

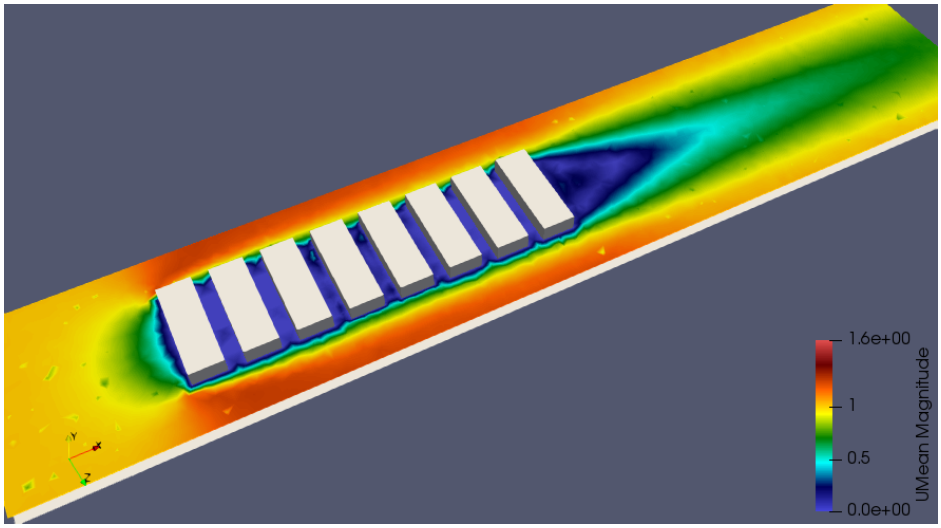

Figure 42: Velocity map at Y = 0.5, (Y normal) when AR = 2

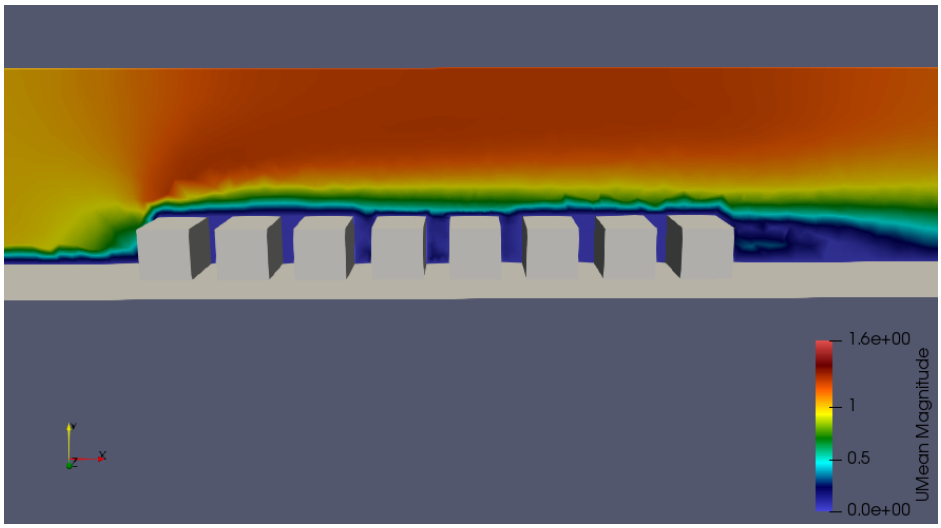

Figure 43: Velocity map at Z = 3, (Z normal) when AR = 2

In figures 42 and 43, the maps shown can be compared with the case where the aspect ratio is one. In general, it can be said that the flow velocities has the same behaviour.

The streamlines are also shown in figures 44 and 45. The same view as in the previous case is going to be shown. This is done this way to ensure that the qualitative comparisons are well presented.

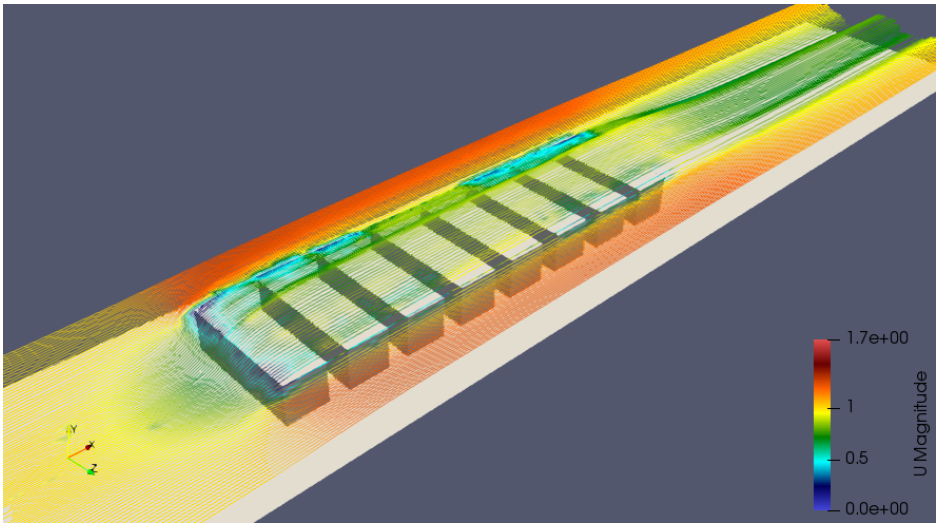

Figure 44: General view of the streamlines in the three dimensional case when AR = 2

From figures 44 and 45, no important difference can be found. Even in the streamlines figures, the behaviour of the air is very similar in general terms as in the previous study. A closer study must be done.

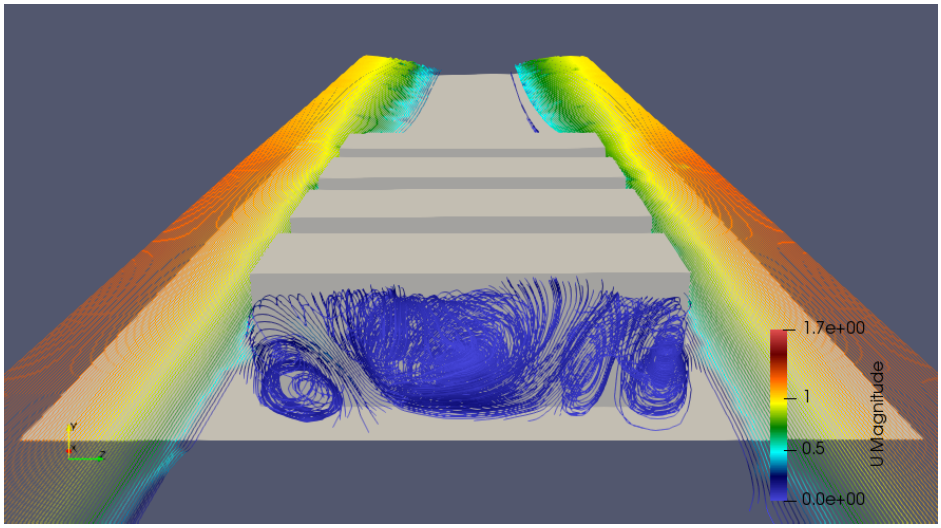

Figure 45: Frontal view of the whirlwind inside the street canyon when AR = 2

5.3.4 Velocity map for the other geometries

Other simulations with aspect ratios between one and two have been made. It is easy to see that the behaviour of the fluid is very similar in all that cases. Comparing all the simulations done, just qualitative conclusions can be taken. For that reason, and to optimize space, no figures will be shown representing the velocity maps or the streamlines of those simulations.

5.3.5 Qualitative results when AR = 1

Some results of the first simulation are displayed here. First, it will be shown a graph where there are a comparison between the flow velocities in the two dimensional case and the three dimensional case. And then, three graphs to see how the flow behaves in the boundaries of the street are shown. But all these are results to make qualitative conclusions.

The comparison graphs between the two dimensional case and the three dimensional case can be seen in figures 46, 47, 48, 49 and 50.

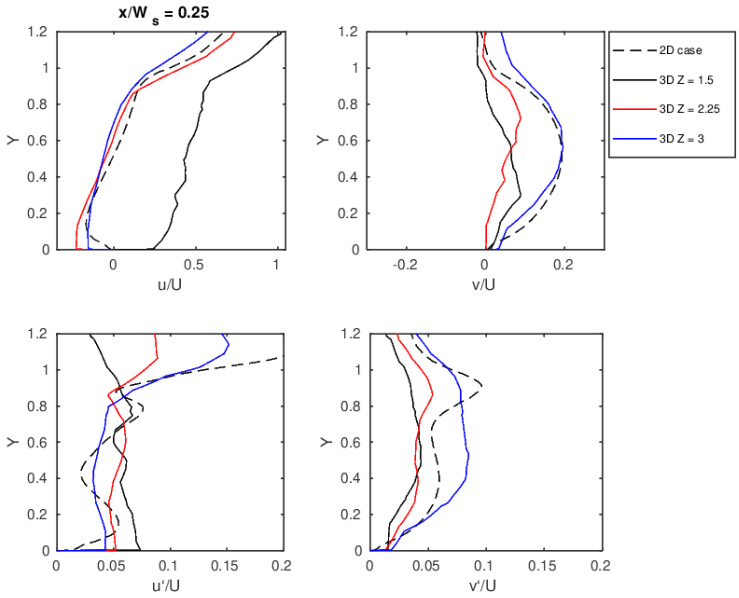

Figure 46: Two dimensional simulation and three dimensional simulation at $X = 12.25$

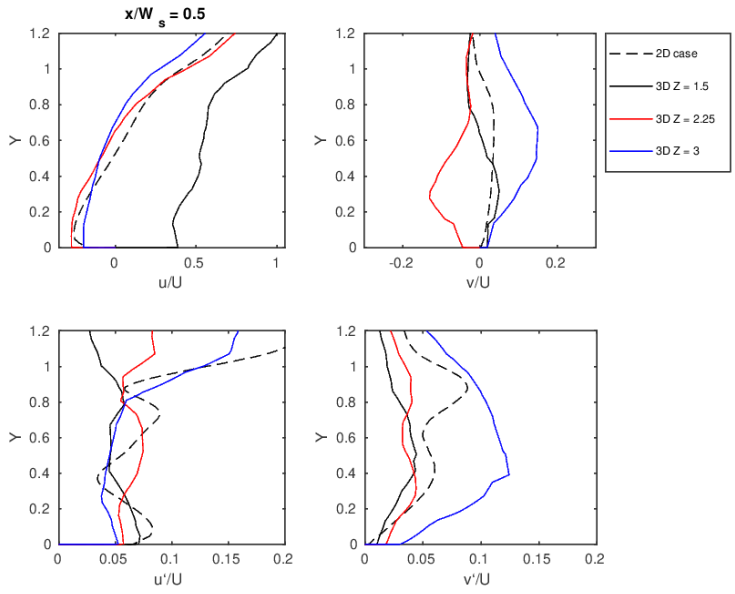

Figure 47: Two dimensional simulation and three dimensional simulation at $X = 12.5$

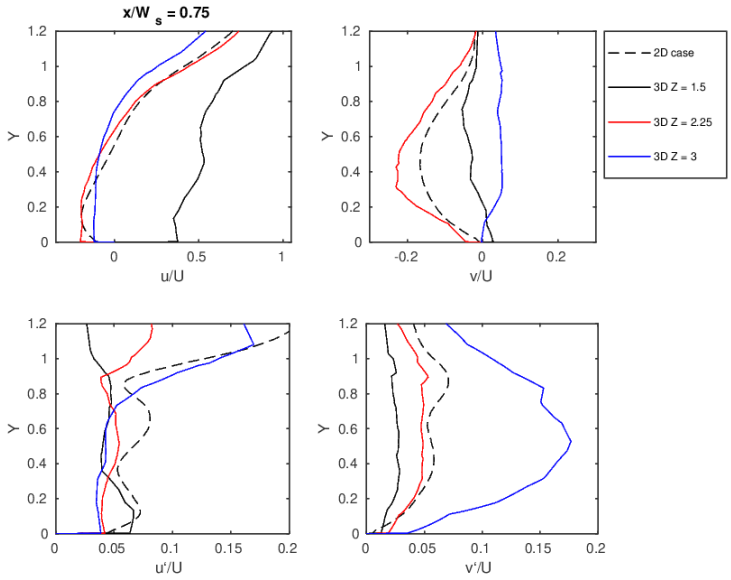

Figure 48: Two dimensional simulation and three dimensional simulation at $X = 12.75$

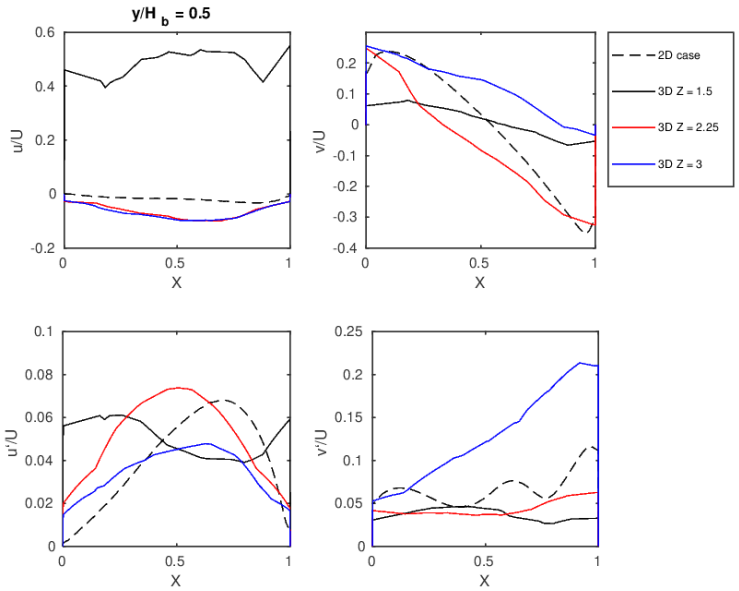

Figure 49: Two dimensional simulation and three dimensional simulation at $Y = 0.5$

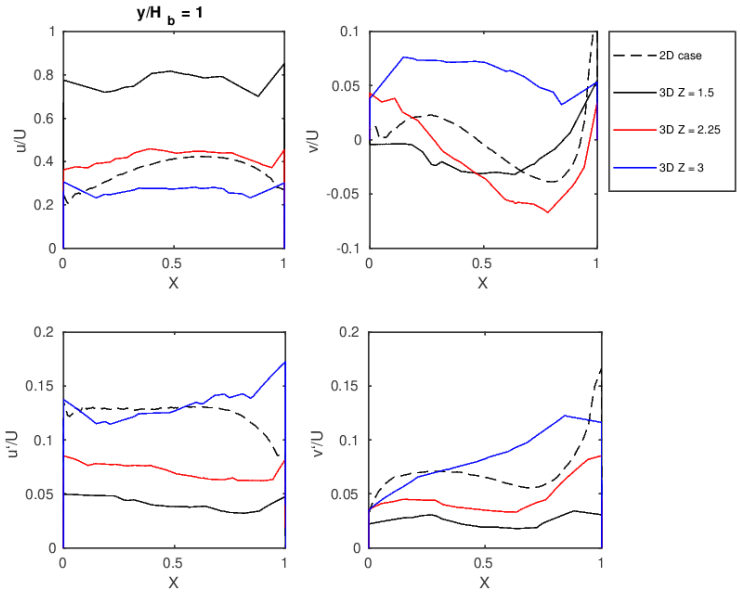

Figure 50: Two dimensional simulation and three dimensional simulation at $Y = 1$

In graphs 46, 47, 48, 49 and 50 the black dashed line refers to the velocities obtained before in the two dimensional case. The other three straight lines are the simulations made with the three dimensional geometry. Each straight line is a measurement in different positions of Z. As the legend of the graphs show, the black straight line is the measurement made in the position $Z = 1.5$, where the street begins. The next one, the red straight line, is taken in the position $Z = 2.25$, between the middle of the street and the end of it. And the blue straight line refers to the measurement made in the middle of the street $Z = 3$.

Taking the measurements on this lines, it is supposed that the flow is symmetric with respect to the $Z = 3$ plane. In the five graphs shown before, the distribution the the four plots are the same as in the two dimensional case. There are represented the mean velocity and the fluctuations in the X and Y directions. Each one divided by the reference velocity.

The following graphs are going to show the velocity that enters and gets out of the street canyon of study. The measures has been taken the following way. It is considered and as it is obvious, that the surfaces where the air can flow are the top of the street and each side. At each surface three

measures will be made. These results are taken to see how the flow behaves in a qualitative way.

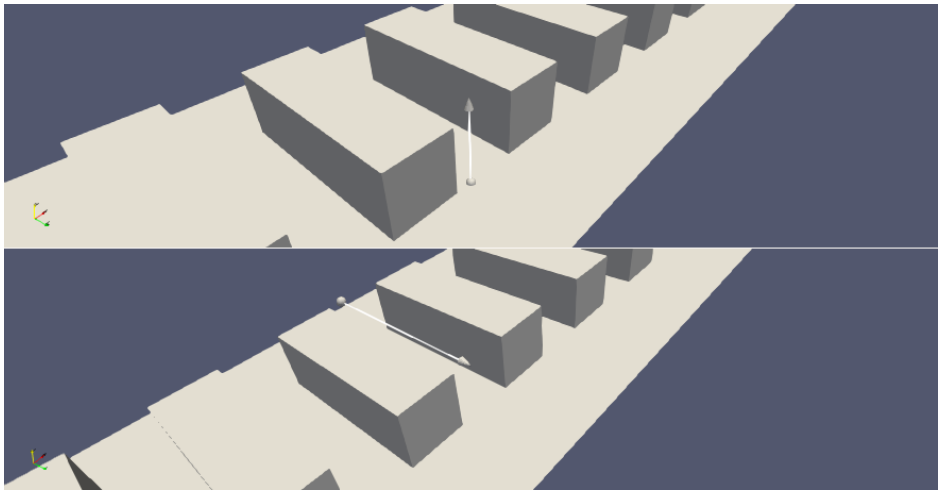

Figure 51: Explanation how the measures are taken, geometry of control. Top: vertical (Y) direction. Bottom: (Z) direction

So, the three measures are located in the longitudinal position of $X = 12.25$, $X = 12.5$ and 12.75. The two ones taken at the sides, cover from the floor, $Y = 0$ to the position $Y = 1.2$. The measures taken a the *ceiling* of the street go see from $Z = 1.5$ to $Z = 4.5$, covering all the length of the street. Figure 51 shows how the results are taken.

In each graph, the black line has been taken in the $X/W_b = 0.25$ position, the red line in the position $X/W_b = 0.5$ and the blue line represents the air velocity in the position $X/W_b = 0.75$. The graphs 52, 53 and 54 shows some interesting aspects of the three dimension air flow distribution that will be explained later.

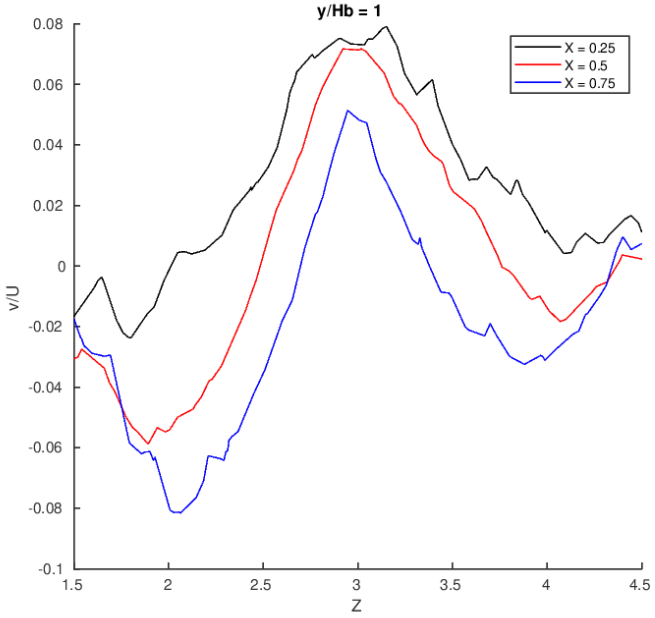

Figure 52: Mean velocity at the ceiling of the street. $Z = 1$

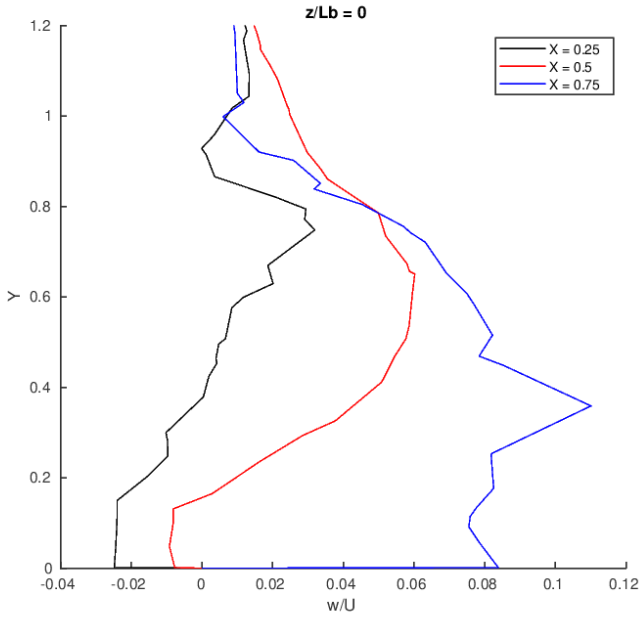

Figure 53: Mean velocity at the left side of the street. $Z = 1.5$

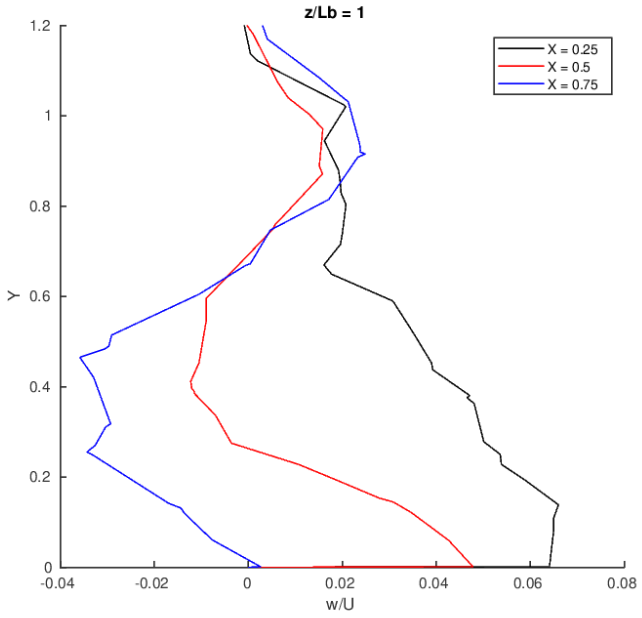

Figure 54: Mean velocity at the right side of the street. $Z = 4.5$

5.3.6 Results of air exchange rate

Now, the graphs to see how the pollution dispersion varies with the buildings geometry are going to be presented. To study it, the air exchange rate is used (ACH). This method will be explained later. To obtain that, the street canyon as a control volume must be considered. Now, the three surfaces where the air can flow are the top and the two sides. The velocity fluctuations in the normal directions of those surfaces are needed.

The graphs showing the fluctuations explained before are the ones in figures 55, 56 and 57.

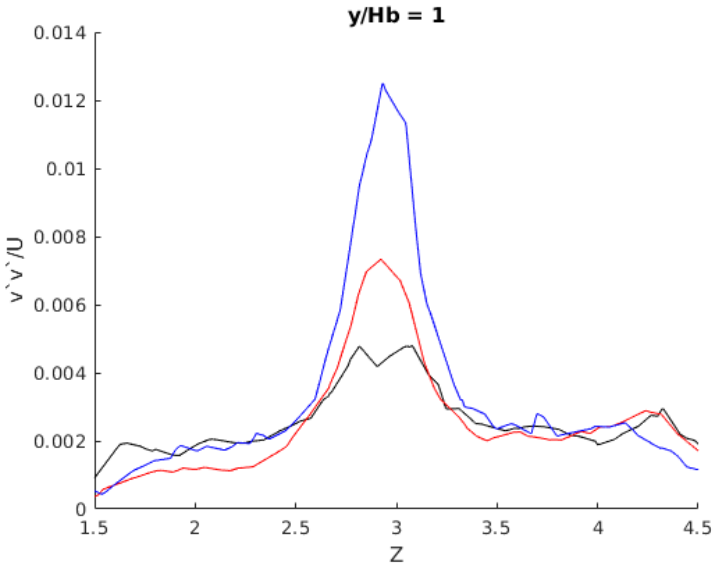

Figure 55: Air fluctuations in the top surface

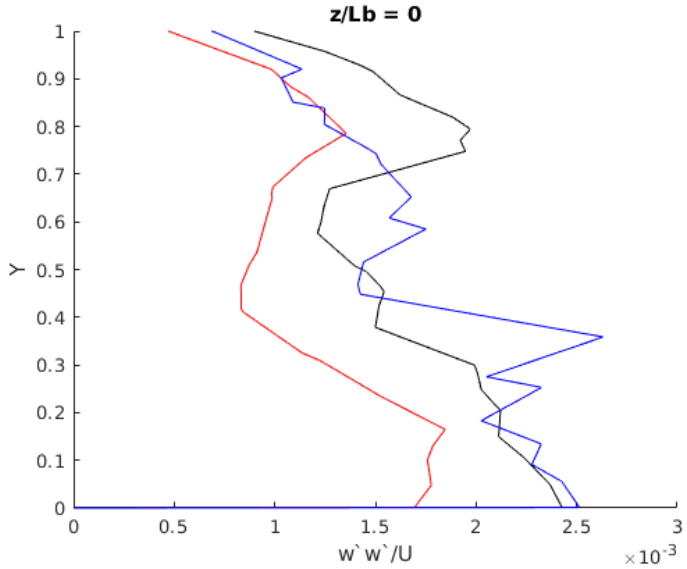

Figure 56: Air fluctuations in the left surface

The measurements presented in figures 55, 56 and 57 have been made in three different points located at the same distance between them. In that case, those points are $X = 12.25$, $X = 12.5$ and $X = 12.75$. But in the following geometries where the street width is shorter, the method is the

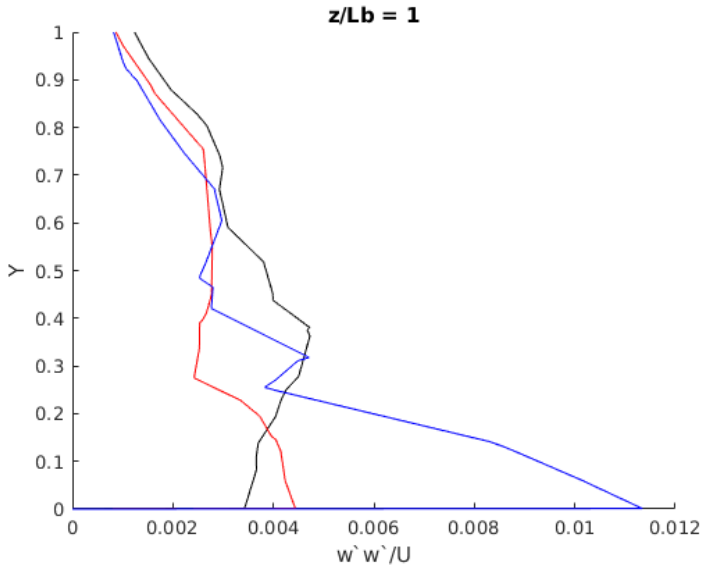

Figure 57: Air fluctuations in the right surface

same, three points dividing the surface in four. The main objective is to find an approximated value of the air fluctuations in the boundaries of the new control volume, the street canyon.

5.3.7 Air exchange rate

The pollutant dispersion and the fresh air introduction to the street must be studied. Because of continuity, those values are the same. To do it, the air exchange rate (ACH) is used. It represents the volumetric air exchange per unit time. The method used is extracted from [11]. To calculate it the following formula is used:

$$\overline{ACH+} = \frac{1}{2}\int_{\tau} \overline{W'W'}^{1/2} d\tau \tag{40}$$

Being τ the distance of the surface taken, in the *ceiling* is the Z direction and in the sides the Y direction. As this formula is used in a two dimensional control volume it has been adapted for the three dimensional case. In the attachments, the MatLab code used to take the data is shown. At each surface, three measures along it has been taken. Then, each measure has been integrated as the formula says and later averaging the results for each surface. The contribution of each surface must be taken into account. A geometrical constrain is that the top surface is three times the surface at the

side. This is because the length and the height of the buildings are constant $L = 3$ and $H = 1$. So if the measure that changes is the width, those surfaces will maintain this relation for the cases studied.

The ACH has been non-dimensionalized by the unity volume V, and the reference time $t = H/U$, where U is the unity velocity and H in the height of the buildings. [11].

Air exchange rate table	
Aspect ratio (H/W)	ACH/(V/t)
1	0.1241
1.25	0.081
1.5	0.0588
1.75	–
2	0.0339

Table 5: Table showing the air exchange ratio for each aspect ratio

As table 5 shows, the simulation with aspect ratio $AR = 1.75$ could not be solved. That is because the simulation was giving convergence problems. It is clear that the origin of the problem has to do with the size of the mesh and the increment of time. It also must be said that the simulation with aspect ratio $AR = 1.5$ has not converged as expected.

Surface of each case	
Aspect ratio (H/W)	Surface (m^2)
1	5
1.25	4
1.5	3.33
1.75	–
2	2.5

Table 6: Table showing the relation between the aspect ratio and the surface of the boundaries of the street canyon

Table 6 is also important, because the objective is to see if the air exchange ratio is proportional to the surface boundaries of the street canyon.

And now, the graphs of the results obtained are going to be presented. First, the relation between the aspect ratio and the air exchange ratio is shown in figure 58.

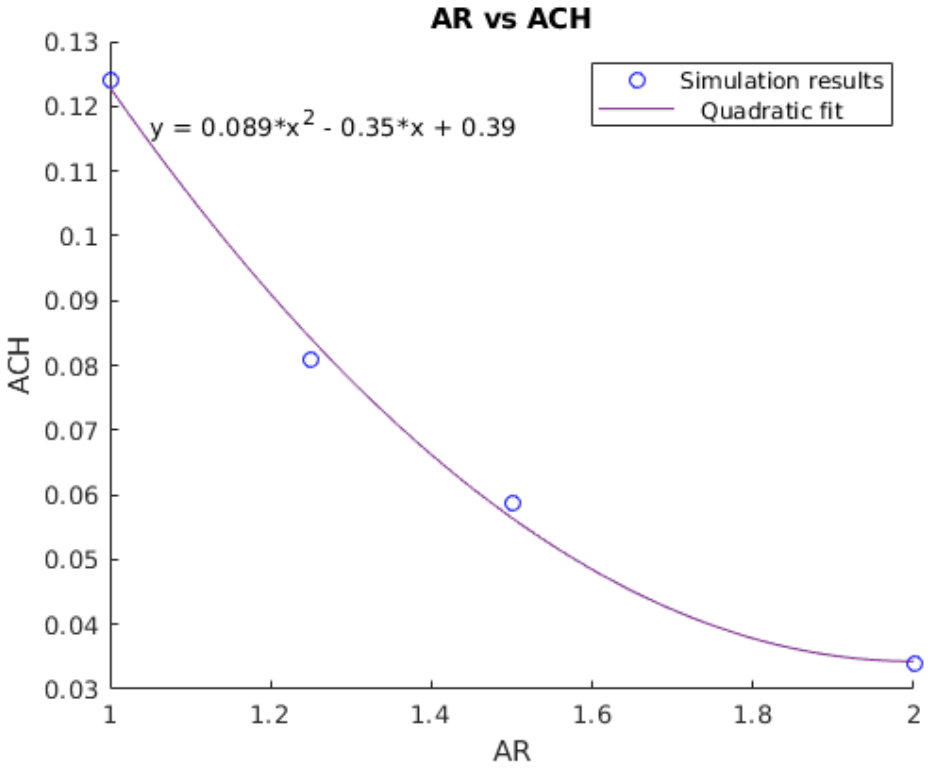

Figure 58: Four results of the simulations. Relation between the aspect ratio and the air exchange ratio and the quadratic fit

As expected, the air exchange decreases when the aspect ratio increases. As the simulation done with aspect ratio $AR = 1.75$ has not been well simulated, just four results are shown. In the graphs 58 and 59, the quadratic fit is used to see how the relation between the parameters should behave in this range of aspect ratios. It is easy to see that the air exchange ratio and the surface of the control volume are almost proportional in this range.

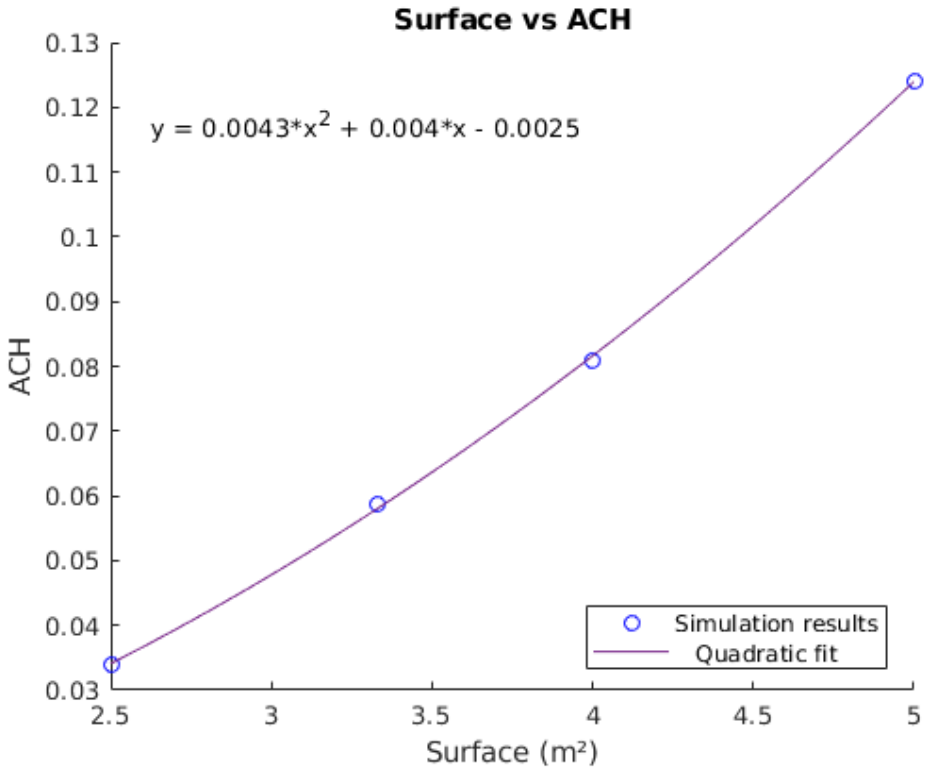

Figure 59: Relation between the surface of the street and the air exchange ratio and the quadratic fit

5.4 Discussion

The discussion will be divided in different parts. First, the three dimensional geometry with aspect ratio $AR = 1$ will be commented. Then a comparative between the two dimensional case and the three dimensional case will be done. Third, the air dispersion rate of the cases simulated with a three dimensional geometry will be compared. From the case with higher aspect ratio, a fewer air dispersion is expected.

5.4.1 Three dimensional case

Looking at figures 52, 53 and 54, an interesting phenomena can easily be seen. The first one, is that in the position $X/W_b = 0.25$ the flow tends to get out of the street through the sides, and the *ceiling*. And in the other side of the street, the opposite phenomena happens. It is easy to see how the blue line, representing the flow velocity in the position $X/W_b = 0.75$ tends to enter the street through the three surfaces. This measures confirms the

inverted U shape of the whirlwind qualitatively stated before.

5.4.2 Comparison with two dimensional case

The qualitative results of the three dimensional flow were expected, it is clear that the whirlwind created is a sum of the swirl known from the two dimensional case and the two new swirls that have appeared from each side. It can be noted that the X component of the velocity in the measures taken in the plane $Z = 1.5$ is higher than in the other planes. This is due to the effect of the velocity of the air that flows around the buildings.

But looking at the graphs, there is a phenomena that was not expected. It is known that the three dimensional case take the effect of the air flowing through sideways of the buildings into account. Then, it is expected that the measures in the middle of the street (in the plane $Z = 3$) are the most *ideal* ones. This means that the middle of the street is the place where theoretically, air velocities approach better the two dimensional case. However, when comparing the two dimensional measures with the three dimensional ones something different is obtained. It can be said that in the plane $Z = 2.25$ (Z normal), the air velocities are also very well simulated, sometimes better that in the plane $Z = 3$ (Z normal). From this, it could be stated that the air flow has an *ideal* behaviour in more than half of the street length.

It can be stated from the qualitative results obtained from the three dimensional simulation that the flow is well represented. The introduction of the flow at each side of the street and the mixing of the eddies are well simulated. I can be said that the velocity results are very similar to the ones in the two dimensional case at some points of the street but the flow obtained is very difficult to define or predict.

The results of the air exchange ratio for the case where the aspect ratio is one can be compared with the literature. The air exchange ratio for a two dimensional geometry with aspect ratio of one is known. The result obtained in the three dimensional case is $ACH = 0.1241$. And the result of the two dimensional case is $ACH = 0.058$ [11]. As it is obvious, the air exchange ratio is higher in the three dimensional case. As a consequence of adding the surface in the sides, the air dispersion increases. Because of the geometry, comparing both cases is very complicated but it can be said that the results are as expected.

5.4.3 Comparison with different aspect ratios

The main aspect to comment is the air exchange ratio. However, other comparisons can be made. For example, it is seen that the shape of the flow streamlines inside the street canyon are very similar in all aspect ratios. The horizontal eddy mixing with the eddy on each side can be seen in every simulation. It is also clear that it is very difficult to reach conclusions by just looking at the velocity map or the streamlines.

The amount of air removed is the same amount of air that enters the street. This is why the heat island effect and pollutant removal are both studied. It is easy to see that the fresh air introduced to the street will have a direct effect on the temperature. Then, for the streets geometries with a low aspect ratio, the pollutant dispersion is high. But as seen in the graphs, the air dispersion changes a lot with the aspect ratio. When the aspect ratio has changed from one to two, the air dispersion has been reduced to a quarter of its value. It can be said from the graphs that the relation of the air exchange ratio and the aspect ratio is not linear. However, a clear relation between the ratio and the surface is found. It can be said that they are proportional for the range of aspect ratio studied.

6 Conclusions

From the two geometry studies performed in this project, some conclusions can be made. It is very important to say that modeling the turbulence is complicated. Each case must be studied in detail, adapting the solver for it. For this reason, a discussion after each case has been done. In this section, the general conclusions of the project are presented.

First, it is important to talk about the main difficulties faced in this project. The learning process has taken longer than expected and the main reason is that the study task required a lot of different learning paths. In the first place, the literature review of previous cases and studies of the air in street canyons. The programs needed for the simulations have also taken a lot of time. And finally, learning about the simulation of fluids, more specifically the $RNGk-\epsilon$ model. As expected, another difficulty found in the thesis was the validation of the model. In order to do it, the results of the simulation had to be compared with the experiments from the literature. A lot of ways were found to reach the k and ϵ parameters, but it is never something exact. That is the reason why the study of six different models are carried out in the validation. The main difficulty of the three dimensional case has been the convergence of the simulations. Different meshes have been created to adjust the element size for the solver.

After validating the model and making all the simulations with the three dimensional geometry, some conclusions can be made. It is clear that for with computer used, which only had one core, the computing power required was a bit high. But in general, it can be said that the RANS model is very efficient, since the most complicated simulations were solved in general after four days. It also gives a good approximation of the results. The $RNGk-\epsilon$ model has given very satisfying results simulating the airflow in street canyons.

The calendar of the thesis proposed in the project charter has been followed with precision. It can be said that the two studies have lasted more or less the same time as said in the Gant's diagram. The error committed at the beginning was the time invested in learning about the programs. A huge amount of time is spent so as to start using three programs from the beginning. A big amount of time has also been invested in watching how the simulations run, especially in the validation of the model, where a lot of values were unknown. During that process, there is no exact way of finding the correct model. Simulating is sometimes a try and error issue.

As it is said before, the computational power and the time running simulations have been a obstacle for the study. Even for RANS models that are faster and more efficient than the LES, for example. So to continue further with the study of pollution dispersion in cities, the optimization of the simulations, even changing the model could be a good measure applied. More simulations with different geometries could be done and even changing the wind direction. It is clear that the results of pollution dispersion would change if the wind direction is 45 degrees with respect of the X direction. Other studies could be done like taking a city where the buildings have the shape of a cube. Other improvements to the study could be increasing the aspect ratio range to see how the air dispersion changes when the buildings are located in more extreme cases.

As some comparisons with a real city must be done, Barcelona has been chosen. First, the neighbourhood *l'Eixample* is taken. Almost every street have a width of 20 meters and a height of 24.4 meters. That makes the aspect ratio of the neighbourhood $AR = 1.22$, very close to the results obtained before for an aspect ratio of 1.25. That means that the pollution dispersion of the neighbourhood *l'Eixample* is almost 0.081. It can be said that the real value is higher for geometrical reasons. The buildings of *l'Eixample* are not squared so the shape of the chamfer will increase the pollution dispersion. But in the neighbourhood of *Gràcia*, for example, the aspect ratio of the streets is more or less 2. In that case the pollutant dispersion is 0.0339. Knowing this it can be said that in this neighbourhood the pollutant dispersion is less than half in comparison with *l'Eixample*.

Finally, it is worth stating that the heat island effect and the pollutant concentration are huge issues in cities. And in the results, it is found that the whirlwinds make the air remain in the street as was expected. But thanks to the model created, a more precise way to study this phenomena is found. This means that new studies can be designed in order to minimize those harmful effects. In the study made, it can be observed that the air dispersion and the street aspect ratio are strongly related. So it can be concluded that the city geometry will have a huge effect on the street atmosphere and therefore on the life of the citizens.

References

[1] T.R. OKE. Street design and urban canopy layer climate. *Energy and Buildings*, 11:103–113, 1988.

[2] T.R. OKE. *Boundary layer climates*. Routledge, 1988.

[3] Chun-Ho Liu Xian-Xiang Li, Dennis Y.C. Leung and K.M. Lam. Physical modeling of flow field inside urban street canyons. *Journal of applied meteorology and climatology*, 47:2058–2067, 2007.

[4] David C. Wilcox. *Turbulence modeling for CFD*. DCW Industries, Inc., 1993.

[5] C.M. Mak Z.T. Ai. Cfd simulation of flow in a long street canyon under a perpendicular wind direction: Evaluation of three computational settings. *Building and enviroment*, 114:293–306, 2017.

[6] C. Foias, O. Manley, R. Rosa, and R.Temam. *Navier-Stokes equations and turbulence*. Cambridge university press, 2004.

[7] Anil W. Date. *Introduction to computational fluid dynamics*. Cambridge university press, 2003.

[8] Giovanni P. Galdi. *An Introduction to the Mathematical Theory of the Navier-Stokes Equation*. Springer-Verlag New York, 1998.

[9] F. Kafyeke E.Laurendeau T. Cebeci, J.P. Shao. *Computational fluid dynamics for engineers*. Horizons Publishing and Springer, 2005.

[10] V. Yakhot and S. A. Orszag. Renormalization group analysis of turbulence. i. basic theory. *Journal of Scientific Computing*, 1(1):3–51, 1986.

[11] Dennis Y.C. Leung Xian-Xiang Li, Chun-Ho Liu. Development of a k-epsilon model for the determination of the air exchange rates for street canyons. *Atmospheric Environment*, 39:7285–7296, 2005.

ANNEX VI – DECLARACIÓ D'HONOR